

#### Available online at www.sciencedirect.com



journal homepage: www.elsevier.com/locate/jmrt



# **Review Article**

# A review on microstructures and mechanical properties of protective nano-multilayered films or coatings



Wenjie Cheng <sup>a</sup>, Jingjing Wang <sup>a</sup>, Xun Ma <sup>a</sup>, Ping Liu <sup>a</sup>, Peter K. Liaw <sup>b</sup>, Wei Li <sup>a,\*</sup>

#### ARTICLE INFO

Article history:
Received 5 July 2023
Accepted 2 October 2023
Available online 5 October 2023

Keywords: Nano-multilayered films Preparation technologies Structures Mechanical properties

#### ABSTRACT

Nano-multilayered films offer a multilayer structure arrangement at several to tens of nanometers. They have hardness, high-temperature oxidation resistance, and low wear rates, making them popular in surface protection fields, such as engineering machinery, cutting tools and molds, and electronic instruments. This paper reviews recent research progress on nano-multilayered films, including their general types, preparation methods, microstructures, mechanical properties, and corrosion resistance. Furthermore, the mechanisms of the high hardness and toughness in nano-multilayered films are analyzed in detail. The future research directions for designing nano-multilayered films with improved strengthening and toughening properties are discussed.

© 2023 The Authors. Published by Elsevier B.V. This is an open access article under the CC BY-NC-ND license (http://creativecommons.org/licenses/by-nc-nd/4.0/).

# 1. Introduction

Thin films, also known as coatings, are a layer of material applied to a surface to change their properties or appearance [1–4]. Today advances in the nanotechnology have allowed for the creation of extremely thin films with specific properties, which has opened up new possibilities in the fields, including aviation [5,6], shipping [7], chemical [8], medical devices [9], and surface protection [10]. However, the disadvantages of poor toughness, oxidation resistance, and low fatigue resistance in the application process can lead to premature failure and reduced service life, limiting their potential applications [11,12]. One effective way to overcome these limitations is to

prepare nano-multilayered films with connected interfaces, appropriate modulation periods, and multi-element components [13,14].

Koehler [15] introduced the concept of nano-multilayered films from a theoretical perspective, predicting that these structures could significantly improve the hardness and elastic modulus of materials. In experiments, Yang et al. [16] demonstrated that nano-multilayered films grown in polycrystalline form had outstanding mechanical properties similar to single-crystal films. Lehoczky et al. [17] prepared Al—Cu nano-multilayered films, showing better strength properties under modulus difference. Subsequently, anomalous increases in the hardness and modulus were observed in other metal/metal systems, such as Cu/Ni [18,19], Ti/Al [20,21], and other binary or

E-mail address: liwei176@usst.edu.cn (W. Li).

<sup>&</sup>lt;sup>a</sup> School of Materials and Chemistry, University of Shanghai for Science and Technology, Shanghai, 200093, PR China

 $<sup>^{</sup>m b}$  Department of Materials Science and Engineering, The University of Tennessee, Knoxville TN 37996, USA

<sup>\*</sup> Corresponding author.

multi-element composition systems, such as amorphous-CuZr/crystalline-ZrN [22], Ti/TiN [23], TiN/AlN–Ni [24], TiAlN/  $Zr_3N_4$  [25], and AlCrN/AlCrSiN [26], to varying degrees. Nanomultilayered films consist of multiple layers of nanoscale thickness, with a much larger surface area than monolithic films of the same thickness. By controlling the material, thickness, and order of different layers and the contribution of interfacial and quantum size effects, excellent tuning of mechanical properties, biomedicine, optoelectronic effects, etc., can be achieved. Nano-multilayered films are widely used in various fields, such as optoelectronic devices, biomedicine, and sensors [27–30].

Fig. 1 displays the microstructures of nano-multilayered films, where two different nanoscale materials are stacked on top of each other in the deposition direction of the film. The thicker layer is called the template layer (Layer A in Fig. 1), and the thinner layer is called the modulation layer (Layer B in Fig. 1). The two adjacent layers form a basic unit and maintain a periodic pattern, whose thickness is the modulation period of the multilayer film ( $\Lambda$  in Fig. 1). Generally, the  $\Lambda$  does not exceed 100 nm. The ratio of modulation layers A and B thicknesses is called the modulation ratio (see Fig. 1).

Regarding classification, nano-multilayered films can be divided into homogeneous and heterogeneous films based on whether the modulation layer having the same intercrystalline structure. They can also be classified into metal/metal, metal/ceramic, and ceramic/ceramic systems depending on the constituent elements of the modulation layer [31,32].

Compared with monolithic films, metal/metal nano-multilayered films exhibit high strength, morphological stability, and excellent resistance to high temperature and fatigue [4]. For instance, Al/Ti nano-multilayered films with thicknesses ranging from 1 to 90 nm were investigated, using electron magnetron sputtering, and the hardness increased with decreasing layer thickness without softening. The high strength mainly originates from the incoherent layer interface

in Fig. 2 [33]. In contrast, Cu/W nano-multilayered films deposited on Si substrates by ion beams showed that moderate temperatures led to significant in-plane residual compressive stresses and increased defects, which degraded the multilayer structures [34]. W/Ti nano-multilayered films were prepared at different temperatures using the discharge plasma sintering technique, and their mechanical properties were found to be dependent on the bonding temperature, with the highest bending strength of 1847 MPa achieved at 1100 °C [35].

Because of their exceptional properties and favorable stability, ceramic materials have become a hot topic in nanomultilayered film research trends. Metal/ceramic nanomultilayered films are formed when a modulation layer in metal/metal nano-multilayered films is designed as a ceramic. For example, Ti/TiN nano-multilayered films were investigated, based on systematic numerical simulations and sputtering experiments [36], and the results showed that the fracture toughness of the 50-layer nano-multilayered films was 82 % higher than that of monolithic TiN while maintaining comparable hardness to the latter. The friction coefficient of AlCrN/Cu nano-multilayered films was significantly lower than that of monolithic AlCrN with the same preparation parameters [37], owing to the surface refined CuO grains formed at high temperatures. MoS<sub>2</sub>/Zr nano-multilayered films were deposited by sputtering [38], and the introduction of Zr resulted in improved corrosion resistance at high temperatures due to the formation of zirconium oxides, a uniform and dense nano-multilayer structure. Lastly, Ag/TaC nanomultilayered films were prepared by magnetron sputtering [39], and the discontinuous films formed when the 2 nm thick Ag sublayer was alternately inserted into the TaC sublayer exhibited a hardness and friction coefficient of ~42 GPa and 0.227, respectively.

Due to the inherent properties of metals, there are limits to their ability to optimize properties, which has led to the increased interest in ceramic/ceramic nano-multilayered

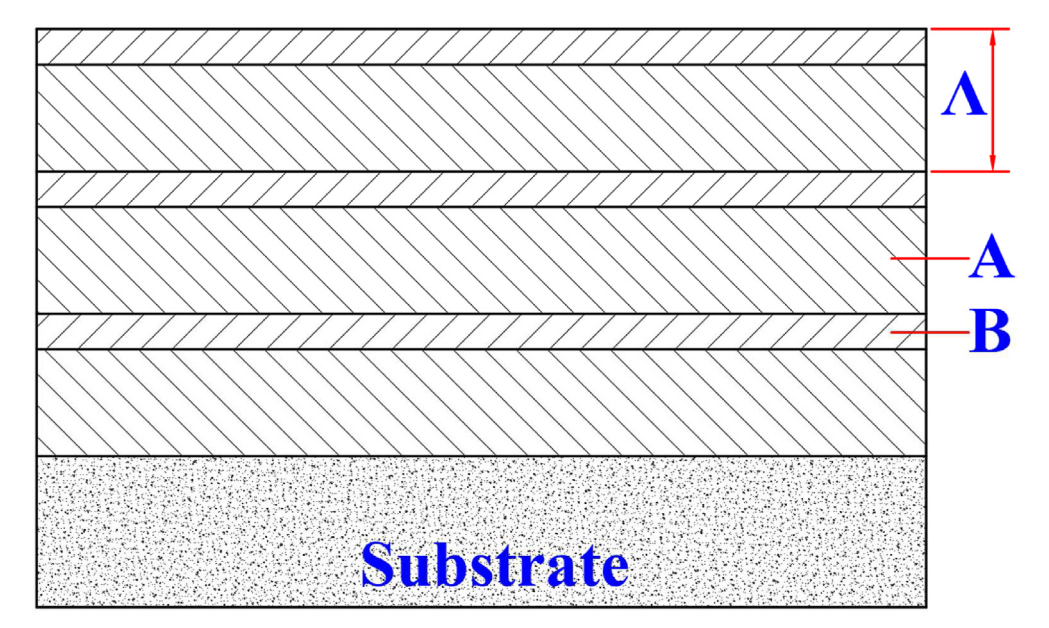


Fig. 1 – Schematic structure of the nano-multilayered film.

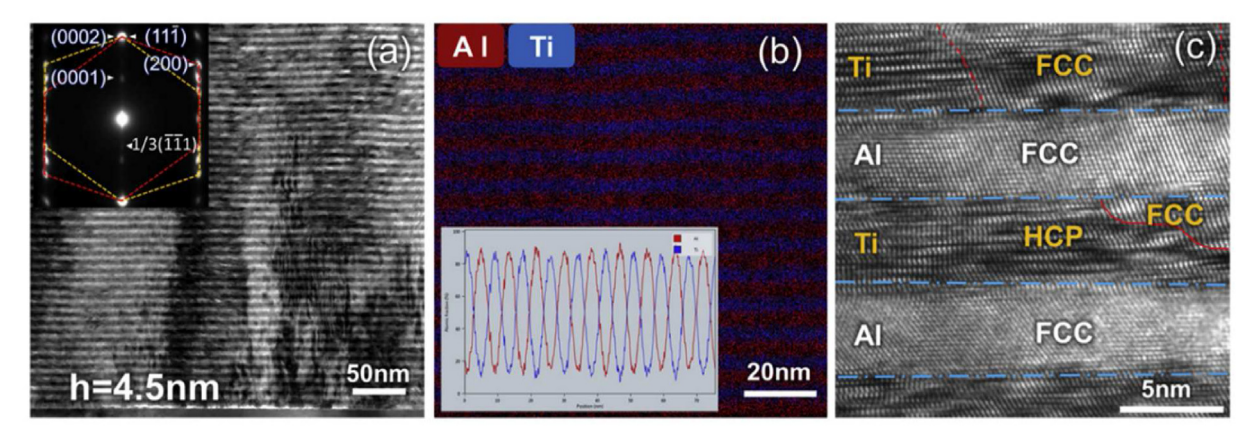


Fig. 2 – XTEM images of Al/Ti Al/Ti layer structure (h = 4.5 nm). (a) Low magnification XTEM and SAD modes. (b) EDS map and line scan of the Al/Ti layer structure. (c) The Ti layer's dual phases [face-centered-cubic (FCC) and hexagonal-close-packed (HCP)] [33].

films. These films have demonstrated superior mechanical properties, compared to selected monolithic ceramic films through non-intrinsic strengthening effects. For instance, Kong et al. deposited CrN/CrCN nano-multilayered films on high-speed steels using cathodic arc evaporation with varying C<sub>2</sub>H<sub>2</sub> flow rates [40]. The films exhibited excellent toughness and adhesion, with hardness and H3/E2 values of 24.3 GPa and 0.176 GPa, respectively, when the C2H2:N2 ratio was 2.5. Additionally, the service life of these films was improved by 33 %, compared to uncoated ones. Similarly, CrN/Si<sub>3</sub>N<sub>4</sub> nanomultilayered films with different Si contents were obtained by magnetron sputtering, demonstrating excellent mechanical properties attributed to a smooth surface morphology, highdensity structure, and favorable nc-CrN/a-Si<sub>3</sub>N<sub>4</sub> interface [41]. Xiao et al. fabricated AlCrN/AlTiSiN nano-multilayered films on cemented carbides and Al2O3 substrates using cathodic arc deposition, presenting a denser two-phase organization with improved hardness and bond strength than AlCrN and AlTiSiN monolithic films [42].

This article covers several topics, including trends and basic types of nano-multilayered films, representative preparation techniques, microstructures, attractive properties, modeling, and simulations. Finally, the review concludes with a summary remark and future research directions.

# 2. Preparation techniques

Nano-multilayered films can be prepared by several techniques, such as physical vapor deposition (PVD) and chemical vapor deposition (CVD) and electrodeposition. PVD includes methods like magnetron sputtering, arc ion plating, etc., while CVD involves atomic-layer deposition, metal-organic chemical vapor deposition, etc. [43,44].

#### 2.1. Magnetron sputtering

Sputtering is a non-heated evaporation process in which the target atoms are bombarded from their surface and deposited onto the substrate by the momentum transfer of high-energy particles. The substrate is not affected by the deposition temperature. Magnetron sputtering is an effective physical

deposition method for preparing nano-multilayered films. The process involves high-speed particles bombarding the surface of a target material (metal or compound) to create a process of sputtering and ionization that results in the formation of layers of nanofilms. The target material is mounted on a target holder in a vacuum chamber, and a substrate is placed in the chamber to receive the sputtered material. The gas in the vacuum chamber is pumped out to maintain a certain vacuum level, and the desired working gas, such as argon, nitrogen, etc., is passed into the chamber to form the ion source. The ions in the working gas are excited by electrodes, magnetic fields, or radiation. Hence, they acquire high energy and accelerate their motion. The ion beam strikes the surface of the target, causing it to sputter and ionize. The sputtered material is deposited on the substrate by the magnetic field, forming a uniform thin film. The advantages of the magnetron sputtering technology are low cost, high productivity, and effective control of the deposition of the ionsputtered material and the properties of the film, making it widely used for the preparation of nano-multilayered films. The principle is shown in Fig. 3. It has two working modes, direct current (DC) and radio frequency (RF). The former works with the metal target and operates independently of the target composition. Both modes can be performed simultaneously if necessary [45-47].

Du et al. used magnetron sputtering to synthesize  $Al_{50}Cr_{50}N/$ Al<sub>80</sub>Cr<sub>20</sub>N nano-multilayered films with different modulationlayer thicknesses [49]. When the modulation-layer thickness was less than 0.9 nm, the film transformed into a FCC structure due to the templating effect of the main layer and maintained coherent epitaxial growth. The films' hardness and elastic modulus reached 39.2 GPa and 356.4 GPa, respectively. ZrO<sub>x</sub>N<sub>y</sub>/ V<sub>2</sub>O<sub>3</sub> nano-multilayered films as a function of N<sub>2</sub>/Ar ratio were fabricated by reactive magnetron sputtering [50]. The K<sub>IC</sub> values increased about 2.15 times when the N<sub>2</sub>/Ar ratio was increased from 5/30 to 20/30, indicating that the reactive gas parameters have an essential role in magnetron sputtering. Villamayor et al. synthesized highly photo-catalytically active layers by combining TiO<sub>2</sub>-nanostructured coatings with 10 nm and 20 nm NiO layers using DC magnetron sputtering [51]. The formation of p-n heterojunctions between the TiO2 layer and

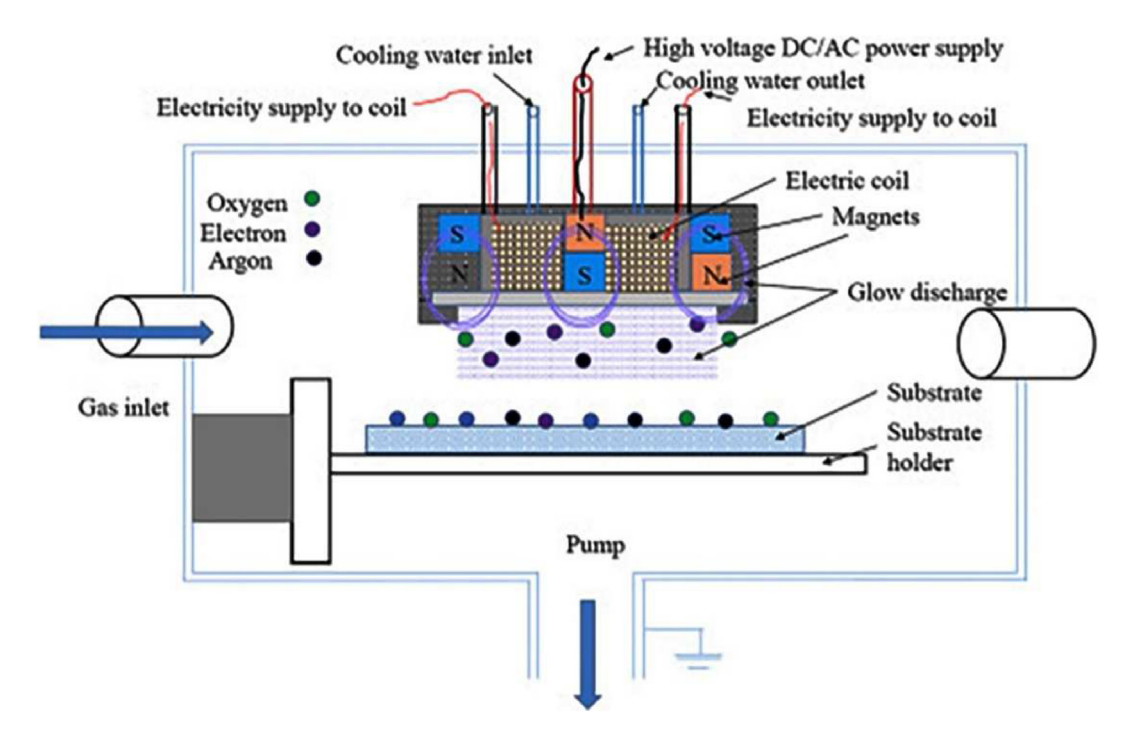


Fig. 3 - Schematic diagram of the mechanism of a magnetron sputter coating machine [48].

the 10 nm NiO layer improved the degradation rate, compared to the bare  ${\rm TiO_2}$  layer. However, there was almost no difference when increasing the NiO-sputtering power and the coating thickness to above 20 nm.

Beltrami et al. deposited two types of nano-laminar coatings, CrN/γ-Mo<sub>2</sub>N and CrN/β-W<sub>2</sub>N, on typical tool steels, using DC magnetron sputtering, and comparatively characterized them [52]. The results showed that improving the nanostructure characteristics of the coatings was beneficial to improve their mechanical behavior and corrosion performance. The thin bilayer cycle CrN/W2N had both the high hardness of β-W<sub>2</sub>N and the excellent corrosion resistance of CrN. The mechanical properties of the CrN/Mo<sub>2</sub>N system were also improved with the thinner bilayer cycle, exceeding the values of the components. Meanwhile, the corrosion performance was better than the single-layer CrN and γ-Mo<sub>2</sub>N coatings. These results suggest that grain refinement obtained by reducing the thickness of the tissue layer is the basis for improving the alloy's mechanical characteristics and corrosion performance. Ku et al. prepared stable epitaxial ZrTiN/ NbN superlattices (SL) using magnetron sputtering. The thickness ratio of ZrTiN to NbN layers was 2.71-0.43 [53]. When the NbN sublayer thickness was more significant than 3 nm, the unstable cubic-NbN transformed to hexagonal-NbN, forming a polycrystalline structure. Due to the nano-laminar structure of ZrTiN/NbN, the hardness and toughness of the multilayer ceramic coatings were improved, compared to the single layer. The nano-scratch showed a step-like curve on the multilayer, the main factor hindering crack expansion. These findings suggest that ZrTiN/NbN is a potentially hard and tough ceramic coating.

The magnetron sputtering technology offers several advantages, such as a fast deposition speed, low ambient temperature, and ease of manipulation. By adjusting the heat-treatment temperature and time after magnetron sputtering, it is possible to obtain nano-multilayered films with varying crystallinity, which facilitates the customization of their properties [44,54]. However, it is essential to note that magnetron sputtering requires a high vacuum and equipment with high hermeticity.

# 2.2. Arc-ion plating

Arc ion plating is a surface treatment process that utilizes arc discharge plasma technology to deposit metal ions on the surface of a substrate, forming a thin film. The process involves using a high-energy arc discharge to generate a plasma that evaporates the metal source and reacts with the ions in the vapor through the ions of the reaction gas, ionizing, and depositing it onto the substrate surface [55,56].

The working principle of arc-ion plating involves heating and evaporating a metal source [e.g., titanium, stainless steel (SS), chromium, etc.] and ionizing it under a vacuum or inert atmosphere using a high-energy arc discharge. Next, the reaction gas (nitrogen, oxygen, argon, etc.) is introduced into the chamber and ionized by the arc discharge. The ionized gas then reacts with the metal ions to form a thin film on the surface of the substrate. The trajectory of the ions of the reaction gas differs from that of the ions in the vapor, generating a strong magnetic field on the substrate surface, resulting in more uniform ionization and deposition.

Arc-ion plating can produce high-quality nano-multilayered films. Fig. 4 shows the working principle of arc-ion plating [57]. The thickness and composition of the deposited layers can be controlled by adjusting parameters, such as the electron energy and current density, and the films can be deposited uniformly in a relatively short time. Moreover, arc-ion plating can introduce various metallic elements and

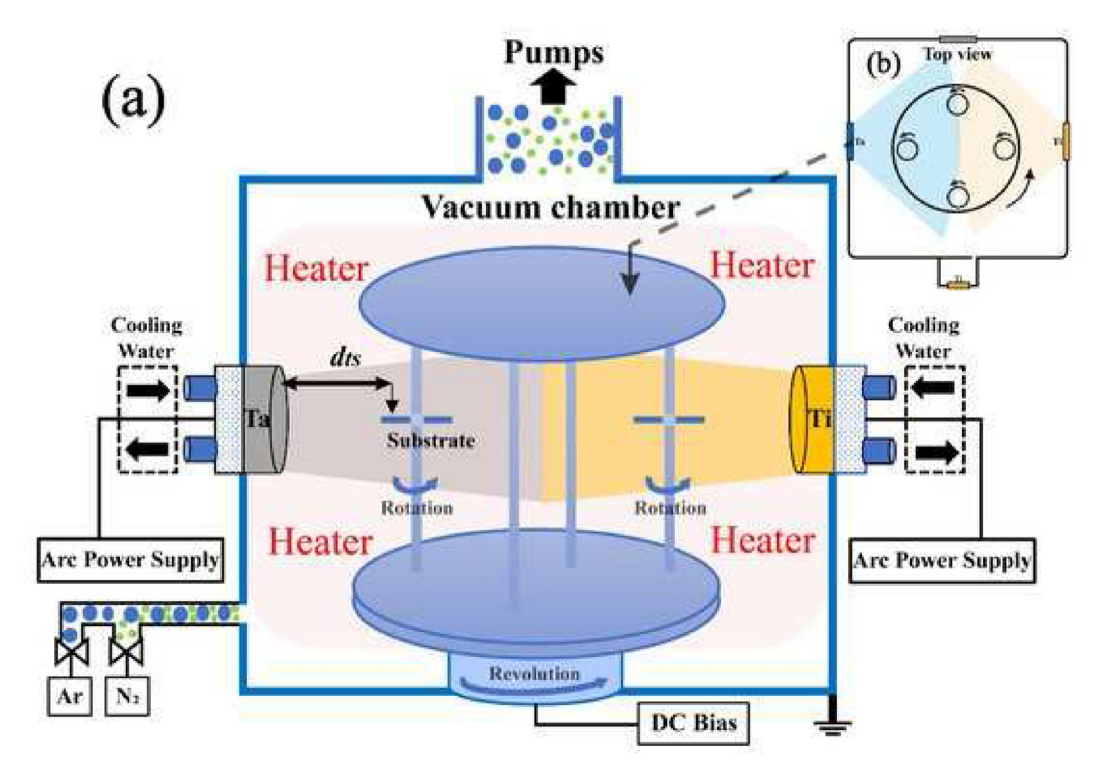


Fig. 4 - Schematic diagram of the multi-arc ion-plating system: (a) front view. (b) top view [57].

compounds into the coating, adding to its unique functionality. Arc-ion plating can form dense and uniform films and improve the wear, corrosion, and high-temperature resistance of material surfaces without changing the properties of the substrate material. Its potential applications include aviation, automotive, machinery manufacturing, electronics, and other fields.

The (Al,Cr)<sub>2</sub>O<sub>3</sub>/ZrO<sub>2</sub>-nano-multilayered films were synthesized on nickel-based high-temperature alloys by arc-ion plating [58]. The resulting alloy demonstrated high resistance to oxidation at 1200 °C due to the formation of the amorphous-Al<sub>2</sub>O<sub>3</sub> phase and interlayer interface in the film, which prevented oxygen diffusion into the interior. The Ti(CuNiZr)N/AlCr(SiW)N nano-multilayered films were also synthesized, using arc-ion plating [1]. The multilayer structure exhibited higher mechanical behaviors with a hardness, H/E,  $H^3/E^2$ , and bond strength of 36.0 GPa, 0.09, 0.291 GPa, and 93 N, respectively. Hu et al. prepared dense and uniform largethickness Cr/CrN multilayer films (≥42 µm) on the surface of the SS by arc-ion plating [59]. The results showed that the Cr/ CrN multilayer film exhibited high adhesion, hardness, and great wear resistance to the steel substrate, compared to the Cr monolayer film. A nitrogen-diffusion phenomenon was also observed, and a solid organic bond formed inside the thick Cr/CrN multilayer film, creating elemental gradients and microstructures. Ma et al. deposited TiAlSiN/TiN multilayer coatings and TiAlSiN monolayer coatings on the surface of the TC18 alloy using a multi-arc ion-plating technique [60]. The adhesion force of the multilayer coating was 62.4 N, while that of the monolayer coating was 51.8 N. Tribological studies indicated that the wear rate of multilayer-coating specimens was 1/7 that of single-layer coating specimens, and this effect was related to the grain refinement caused by the multilayer structure in the coating.

#### 2.3. Chemical-vapor deposition

Chemical vapor deposition (CVD) is a process where multiple reactants undergo a chemical reaction, leading to the deposition of thin films on material surfaces. This process is commonly used to prepare nano-multilayered coatings with various properties and is widely applied in functional, anticorrosion, and optical coatings, among others. The working principle of CVD consists of two main steps: reactant delivery and surface deposition, as shown in Fig. 5 [61]. First, specific reactants, such as gas or liquid, are introduced into the reaction chamber. Under high-temperature conditions, these reactants undergo chemical reactions and decompose into high-activity intermediates. These intermediates are then transported to the surface where the deposition occurs. Through processes, such as adsorption and diffusion, solid deposits are formed on the surface, initiating the formation of the first nanolayer of the individual coating. This process is continuously repeated to create a clear interface between each nanolayer, and finally, the desired thin film is formed. In summary, the chemical-vapor deposition technology utilizes chemical reactions and gas-diffusion principles to prepare nano-multilayered films by heating and transporting the reacting material to the substrate surface.

The thermal-shock resistance of monolithic TaC films and SiC/TaC/SiC/TaC multilayered films were compared by a CVD process using an arc heater [62]. As a result of the SiC layer oxidation, the multilayer structure showed a protective amorphous coating, and the porous  $Ta_2O_5$  layer protected the

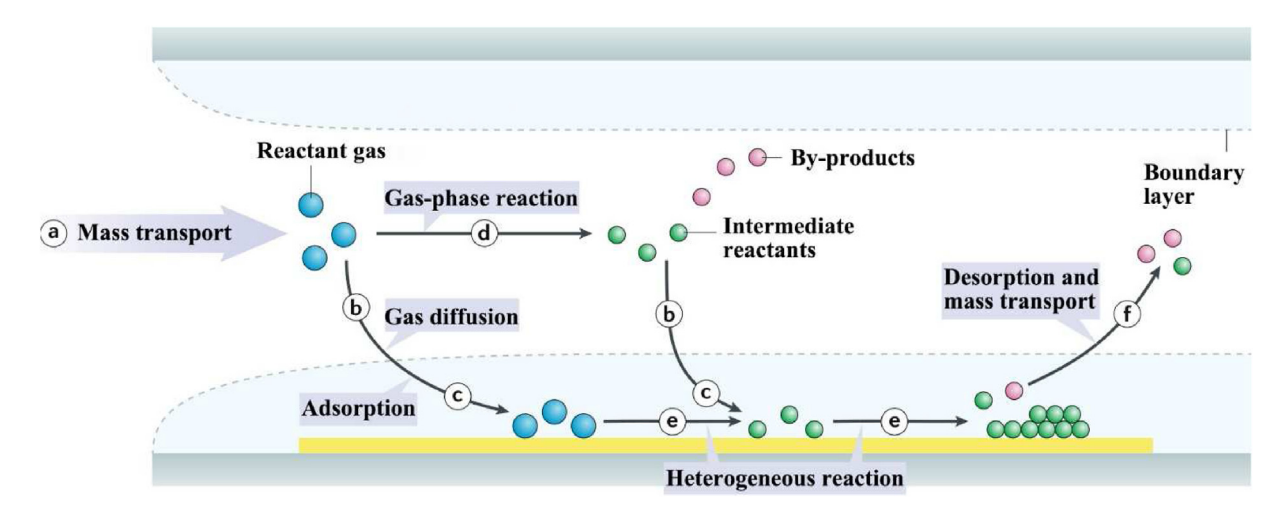


Fig. 5 - Schematic of general elementary steps of a typical CVD process [61].

internal C/C. The MoS<sub>2</sub>/WS<sub>2</sub> heterostructures on SiO<sub>2</sub>/Si substrates were prepared using the CVD process [63]. The results demonstrated that MoS<sub>2</sub>/WS<sub>2</sub> thin films were promising heterostructure materials. The optical responsiveness of multilayer MoS<sub>2</sub> field-effect transistors was improved by more than 50 times using MoS<sub>2</sub>/WS<sub>2</sub> heterostructures as the channel material for phototransistors. The TiN/TiBN multilayered films with A values of 1400, 800, 300, and 200 nm were prepared, using the thermal CVD [64]. The results showed that reducing the A value contributed to the grain refinement and increased the hardness of the multilayered film. The hardness was elevated from 28 GPa to 31 GPa. TiN/MT-TiCN/Al<sub>2</sub>O<sub>3</sub>/ TiCNO multilayered films were fabricated on the cemented carbide by CVD [65]. The results showed that micro-blasting significantly reduced the surface roughness and transformed the residual tensile stress into compressive stress. The film friction coefficient was reduced, and the residual compressive stress increased the hardness and adhesive strength. The epitaxial superconducting (Nb,Ti)N films were deposited, using a CVD technique with an in situ production of precursors, as presented in Fig. 6 [66]. The results demonstrate that the composition of the films is controlled by the chemical composition of the gas phase, and the cubic phase (Nb,Ti) is the thermodynamically stable phase from 800 °C to 1300 °C under the classical CVD. Hexagonal (Nb,Ti)N is formed by a "nitride-like" process under reactive CVD up to 1200 °C. This technique allows to control the superconducting properties of the film by controlling the Ti composition.

PVD and CVD are two commonly used techniques for thin film formation. PVD involves converting a solid material into a gaseous state through physical means, such as ion bombardment or thermal evaporation, and depositing it onto a substrate. The resulting film composition is comparatively controllable. PVD requires high vacuum conditions, leading to high equipment costs. CVD utilizes a chemical reaction to produce a gaseous precursor for forming a thin film on the substrate, which performed at higher temperatures. The chemical reaction process may produce incompletely degraded by-products, such as toxic gases, which require a subsequent treatment. Additionally, due to the high-temperature diffusion of atoms, the interfaces between sublayers in CVD coatings are

usually not sharp, which is beneficial to improve the adhesion between the layers. Finally, the CVD process has a slower deposition rate than the PVD.

#### 2.4. Electrodeposition

Electrodeposition is a traditional surface modification method to improve materials' surface, decorative, and functional properties. Its principle is illustrated in Fig. 7 [67]. Electrodeposition involves the reduction of charged metal ions to metal deposits on the surface of a conductive substrate through an electrochemical reaction to form a layer-by-layer coating. The multilayer structure of the coating can be controlled by adjusting parameters, such as the electrodeposition time, current density, and electrolyte formulation [68,69].

The process involves selecting a suitable conductive substrate material, for example copper or SS, for the surface finish and cleaning treatment. The cathode is usually the substrate material for the film to be prepared, while the anode is used to provide metal ions. The electrolyte is then prepared by selecting a suitable electrolyte according to the coating requirements, such as an acidic, alkaline, saline solution, copper sulfate, or nickel-salt solution. Additives are added in a particular proportion to control the structures and properties of the coating. Next, the electrodeposition parameters are adjusted to set appropriate values, for instance, the electrodeposition time, current density, and temperature, to achieve the desired coating thickness and multilayer structure. The film is grown by continuously reducing metal ions to the metal on the cathode surface, gradually reaching the desired thickness. The multilayer coated substrate, after electrodeposition, is usually washed and dried to make its surface smooth and uniform. This process can prepare multilayer nano-coatings with a high nano-level thickness control, excellent corrosion resistance, and high-temperature oxidation resistance. An electrodeposition technology has the advantages of high efficiency, low cost, and easy control, making it widely used in preparing various thin metal and alloy films in microelectronics, sensors, optics, and biomedical fields.

The Ni–Co–P multilayer films were prepared using pulsed electrodeposition with a cathode duty cycle ranging from 20 %

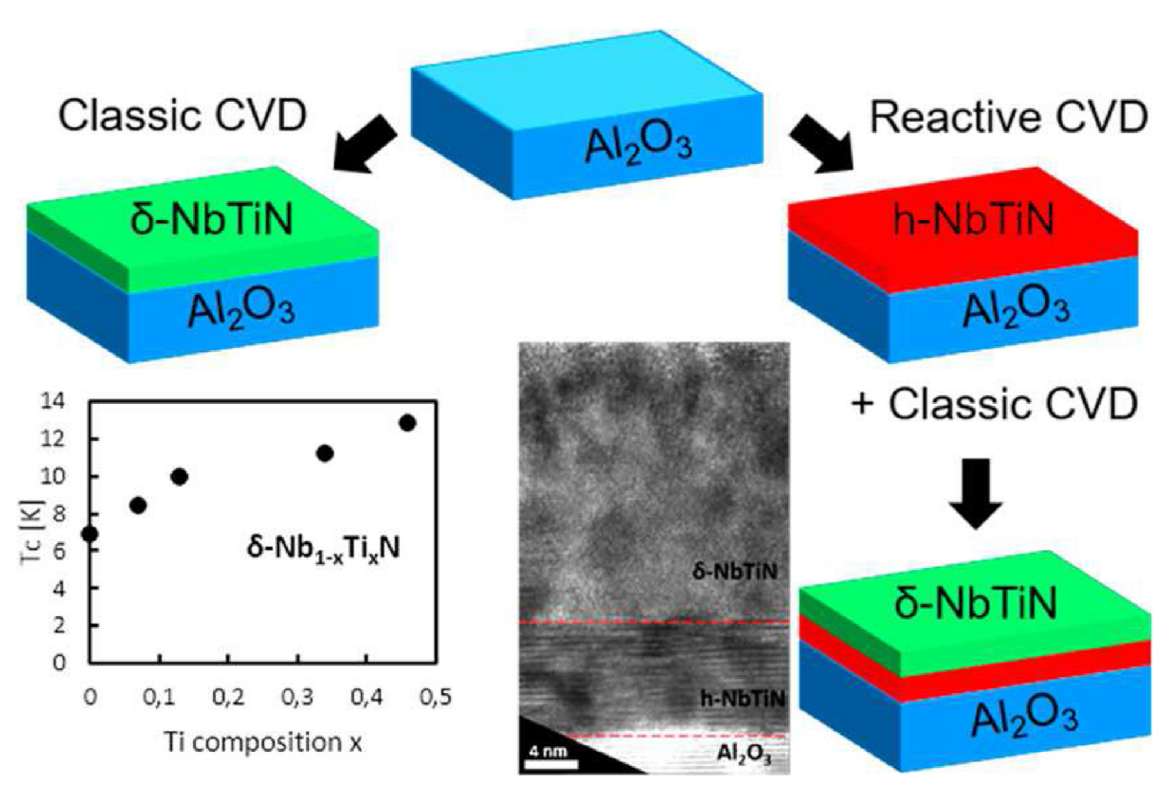


Fig. 6 – Schematic illustration for the formation of hexagonal-(Nb,Ti)N and cubic-(Nb,Ti)N thin films by reactive and classic CVD processes [66].

to 90 % [70]. The results indicated that as the thickness decreased, the microhardness of the films could be enhanced up to 700 HV, and the friction coefficient was reduced to 0.4. The CoMnP/Cu multilayer films were prepared, using the electrodeposition technique on Cu substrates with layer numbers ranging from 2 to ~20 μm total thickness [71]. As the number of layers increased,  $\sigma_{XRD}$  (XRD for the apparent crystallite stress) decreased by 8.3 %, 25 %, and 33 %, and  $\sigma_f$  (curvature-measurement methods for the macro-stress) increased by 7.7 %, 15 %, and 23 %, respectively. The significant reduction of residual stresses contributes to the durability of multilayer films. The electrodeposited Cu/Ni multilayer composites were tested in room temperature tension at strain rates of  $5 \times 10^{-5}$  to  $5 \times 10^{-2}$  s<sup>-1</sup> [72]. The experimental results suggested that the back stresses generated at the interlayer interface increased with the increase of the strain rate and exhibited a solid work-hardening phenomenon, resulting in the excellent plasticity of Cu/Ni multilayer composites. However, one limitation of the electrodeposition technique is the potential for complexity and undesired surface reactions when transferring the substrate between the two electrolytes.

Table 1 shows the different deposition techniques for nanomultilayered films. When discussing the different deposition techniques for nano-multilayered films, it is essential to consider the impact that various factors can have on the specific shearing properties of the films. These factors include target impurities, deposition rates, growth morphology, structural defects, and residual stresses. It is also important to note that the film-preparation technology directly affects the morphology, roughness, and other characteristics of the film

surface, which can ultimately impact its performance and stability in its intended application.

### 3. Microstructures

Variations in microstructures significantly impact the performance of nano-multilayered films, including the  $\Lambda$ , modulation ratio, and material composition. The films comprise multiple nanometer-thick sublayers, typically a few nanometers to tens of nanometers thick. These sublayers can be different forms of the same material or layers of different materials. At the microscopic level, the structure of a nanomultilayer film consists of a plurality of nanograins stacked together. The grains in each sub-layer have similar sizes and shapes, bonded through high-energy grain boundaries with a high dislocation density and plastic-deformation capacity. Due to the larger surface area of the multilayer structure, the atomic arrangement and crystal structure at the interface play a crucial role in the physical and chemical properties of the film. The type and orientation of the crystal structure in films determine their mechanical and physical properties, affecting plastic-deformation behavior in metallic films. Nano-multilayered films can have either periodic or random structures, with periodic structures having better optical reflection and transmission properties and higher physical stability.

However, the microstructures of nano-multilayered films include various defects and impurities, such as voids, dislocations, and heterogeneous structures, which can affect the

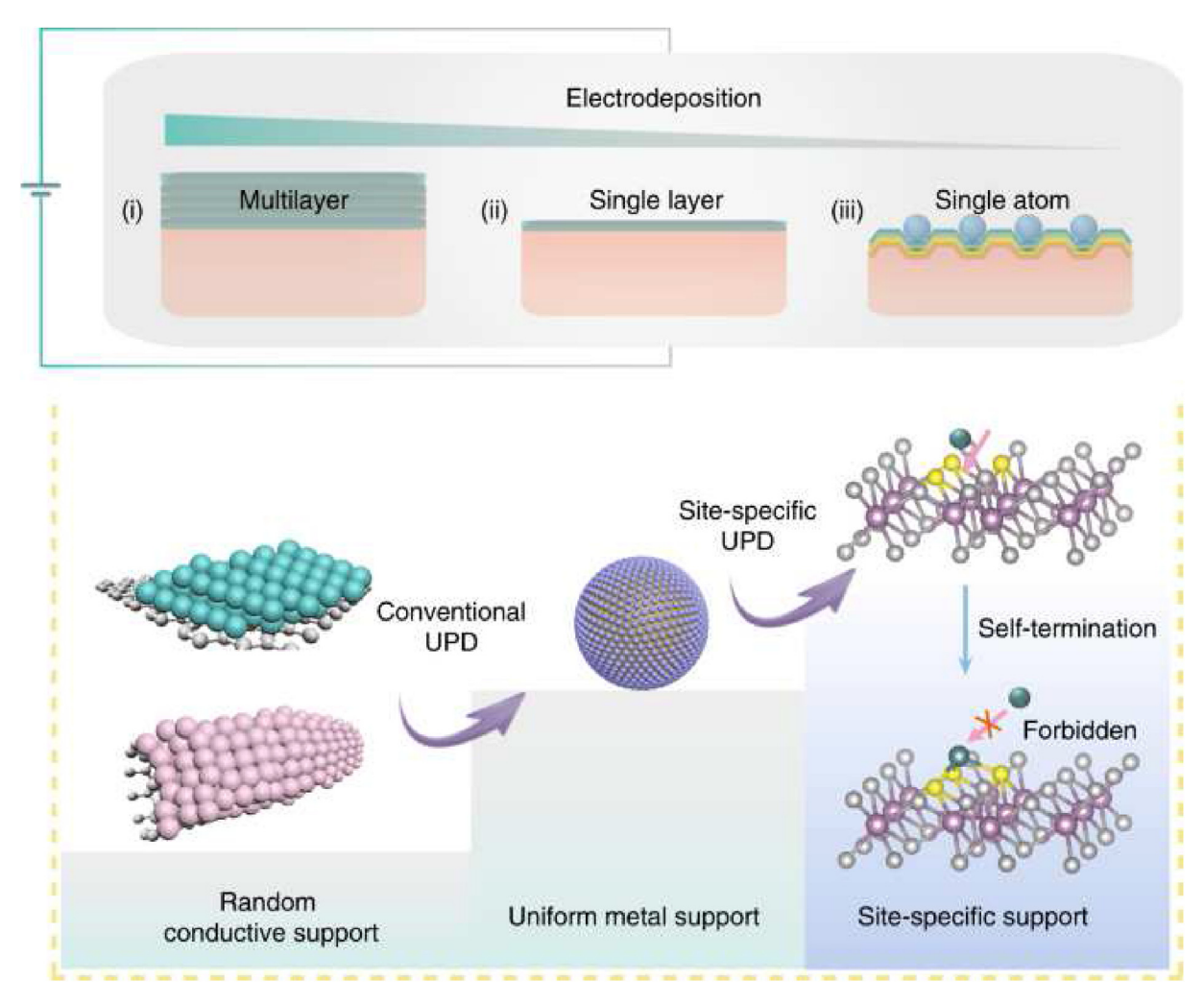


Fig. 7 – Methodological development of atomically dispersed metal catalysts preparation by electrodeposition [67].

Table 1 – Compilation of several na	nno-multilayered films classified according to the composition	and preparation method.
Composition	Preparation method	References
Cu/W	Ion-beam deposition	[34]
AlCrN/Cu	arc ion plating/magnetron sputtering	[37]
CrAlN/CrN	arc ion plating	[73]
Cr/CrN	arc ion plating	[59]
Ni-Co-P	electrodeposition	[70]
CoMnP/Cu	electrodeposition	[71]
Cu/Ni	electrodeposition	[72]
Ti/TiAlN	arc ion plating	[74]
CrN/TiSiN	arc ion plating	[75]
TiAlN/CN <sub>x</sub>	magnetron sputtering	[76]
TiAlN/AlN	magnetron sputtering	[77]
TiMoN/Si <sub>3</sub> N <sub>4</sub>	magnetron sputtering	[78]
T-MLG/Ni	chemical vapor deposition	[79]
WC/Co	chemical vapor deposition	[80]
WSe <sub>2</sub> /In <sub>2</sub> Se <sub>3</sub>	electron beam evaporation	[81]
$Ti_3C_2T_x$	electro spraying	[82]
CeO <sub>2</sub> /ZrO <sub>2</sub>	sol gel	[83]
HfO <sub>2</sub> /ZnO and TiO <sub>2</sub> /ZnO	Atomic layer deposition	[84]

films' mechanical, electrical, and optical properties. Therefore, understanding the microstructures of films requires considering various factors comprehensively. In conclusion, the microstructures of films are a complex system, and its properties and behavior depend on multiple factors, including the sublayer thickness, material composition, crystal structure, and defects.

#### 3.1. Modulation period

Although nano-multilayered films prepared from different materials or processes often have various optimal  $\varLambda$ , deviations from this optimal value can result in unfavorable conditions for preparing high-quality films. Specifically, if the  $\varLambda$  is too large, dislocation shifts may occur in the modulation layer, whereas if it is too small, interdiffusion of grain boundaries or effective segregation may not occur. Thus, obtaining the optimum  $\varLambda$  is crucial for preparing nanomultilayered films with excellent properties.

It has been observed that when the optimal  $\Lambda$  is achieved, two adjacent sublayers of the nano-multilayered films grow together at the grain boundaries, resulting in what is known as "SL films" [85,86]. For example, Liu et al. prepared AlTiSiN/ AlCrSiN nano-multilayered films with different 1 using arcion plating [87]. They found that the hardness increased from 23.9 GPa to 31.6 GPa as  $\varLambda$  was reduced from 147 nm to 60 nm. Similarly, Kravchenko et al. fabricated (Al<sub>50</sub>Ti<sub>50</sub>)N/ZrN nano-multilayered films with different  $\Lambda$  using arc deposition [88]. They observed that the same lattice structure of FCC-(Ti, Al)N and B1-ZrN contributed to the epitaxial growth of the sublayers. The films obtained a maximum hardness of 26.5 GPa, when  $\Lambda$  was decreased to 15 nm. Yan et al. deposited a series of TiAlN/AlN multilayers with different thicknesses of AlN layers on the 304 SS by a magnetron sputtering system [77]. When the AlN layer was 3.2 nm, the TiAlN/AlN multilayers showed excellent performance with a hardness of 30.98 GPa, a roughness of 20.2 nm, and a friction coefficient of 0.61. Zuo et al. investigated the effects of  $\Lambda = 2-36$  nm on the microstructure, mechanical properties and corrosion resistance of TiN/AlN multilayer films [89]. The results showed that the hardness and corrosion resistance of the films gradually increased, as  $\Lambda$  ranged from 2 to 12 nm. When  $\Lambda=12$  nm, the best hardness was 29.27 GPa, while the film obtained the strongest corrosion resistance. With  $\varLambda$  from 26 nm to 36 nm, the coherent interface of the film may be disrupted, and the alternating stress field as well as the hardness decreased sharply.

Overall, the mechanical behavior of nano-multilayered films typically exhibits extreme values when the  $\varLambda$  falls within the range of several to more than 10 nm.

# 3.2. Phase transformations

Nano-multilayered films are composed of many thin films stacked on each other, with modulation periods typically less than 100 nm. When the thickness of the modulation layers or the materials or their ratio changes, a phase transition may occur, disrupting the original crystal structure and causing a new crystal structure to appear. This phase transition can cause changes in the physical and chemical properties of the

film, such as the electrical conductivity, magnetic properties, and optical properties, making it essential for materials science and engineering applications. Additionally, ambient temperature, pressure, humidity, and other factors can also affect the occurrence of phase transitions.

The ZrN/Zr<sub>0.63</sub>Al<sub>0.37</sub>N nano-multilayered films with various modulation layer thicknesses were fabricated on MgO(001) substrates using magnetron sputtering at 700 °C [90]. The films showed the maximum fracture toughness by indentation when the modulation layer thickness was 2 nm in Fig. 8. Then, the metastable crystalline-ZrN (c-ZrN) phase transformed into wurtzite-AlN (w-AlN). When the modulation layer thickness was increased to 10 nm, the w-AlN was semi-coherent with c-ZrN, and the films obtained the maximum hardness value of 34 GPa, which was about 31 % higher than that of the monolithic ZrN. In another study,  $Fe_{1-x}Mn_x$  (x = 0, 0.18, and 0.35)/ TiB<sub>2</sub> nano-multilayered films were prepared, using magnetron sputtering [91]. The moderate addition of Mn to Fe formed a metastable FCC phase, which transformed into the bodycentered-cubic phase under nanoindentation. The fracture toughness of Fe<sub>0.82</sub>Mn<sub>0.18</sub>/TiB<sub>2</sub> was about twice that of Fe<sub>0.65</sub>Mn<sub>0.35</sub>/TiB<sub>2</sub> and Fe/TiB<sub>2</sub>. In an in-situ microcolumncompression experiment, the Ti sublayer of the Al/Ti multilayer film transformed from the HCP to FCC phase with a compressive strength of 2.4 GPa, and the film showed excellent work-hardening ability [92].

#### 3.3. Interfaces

Unlike bulk composites, nano-multilayered films contain multiple interfacial structures, where the bulk fraction determines the properties. Coherent, semi-coherent, and incoherent interfaces are present in these films, and the interfacial structure affects their material properties, such as high strength, fracture toughness, and fatigue resistance [31].

A coherent interface is formed when two modulated layer phases of the multilayer films have the same atomic configuration, and the two crystals are perfectly matched in the orientation at the interface [93]. The effect of the coherent growth model on the hardness of the VN/TiB2 multilayers was shown in Fig. 9. When  $t_{VN}$ : $t_{TiB2}$  (t, thickness) was 7:1, the TiB<sub>2</sub> layer induced crystallization and maintained the same crystal structure as VN. The results showed that the hardness and elastic modulus of the nano-multilayered film achieved 41.8 GPa and 492 GPa, respectively. Meanwhile, the VN/TiB<sub>2</sub> multilayer experiment verified the deduction by the coherent growth model. Du et al. [94] investigated the mechanical properties of TiN/CrN multilayers with modulation periods of 17.8 nm and 6.7 nm, respectively. The results showed that the reinforcement effect induced by the coherent interface increased the hardness from 27.5 to 29.4 GPa.

The strain induced by coherent interfaces raises the total energy of the system. Semi-coherent interfaces, where periodic dislocations occupy the mismatch sites, are energetically more favorable for sufficiently large atomic mismatches or interface areas. The semi-coherent interface has a significant lattice mismatch, resulting in low shear resistance. Fig. 10 shows the rod-like  ${\rm Al_2O_3/GdAlO_3(GAP)}$  eutectic organization perpendicular to the growth direction [95]. The rod-shaped GAP phase formed internally to the orthorhombic GAP phase

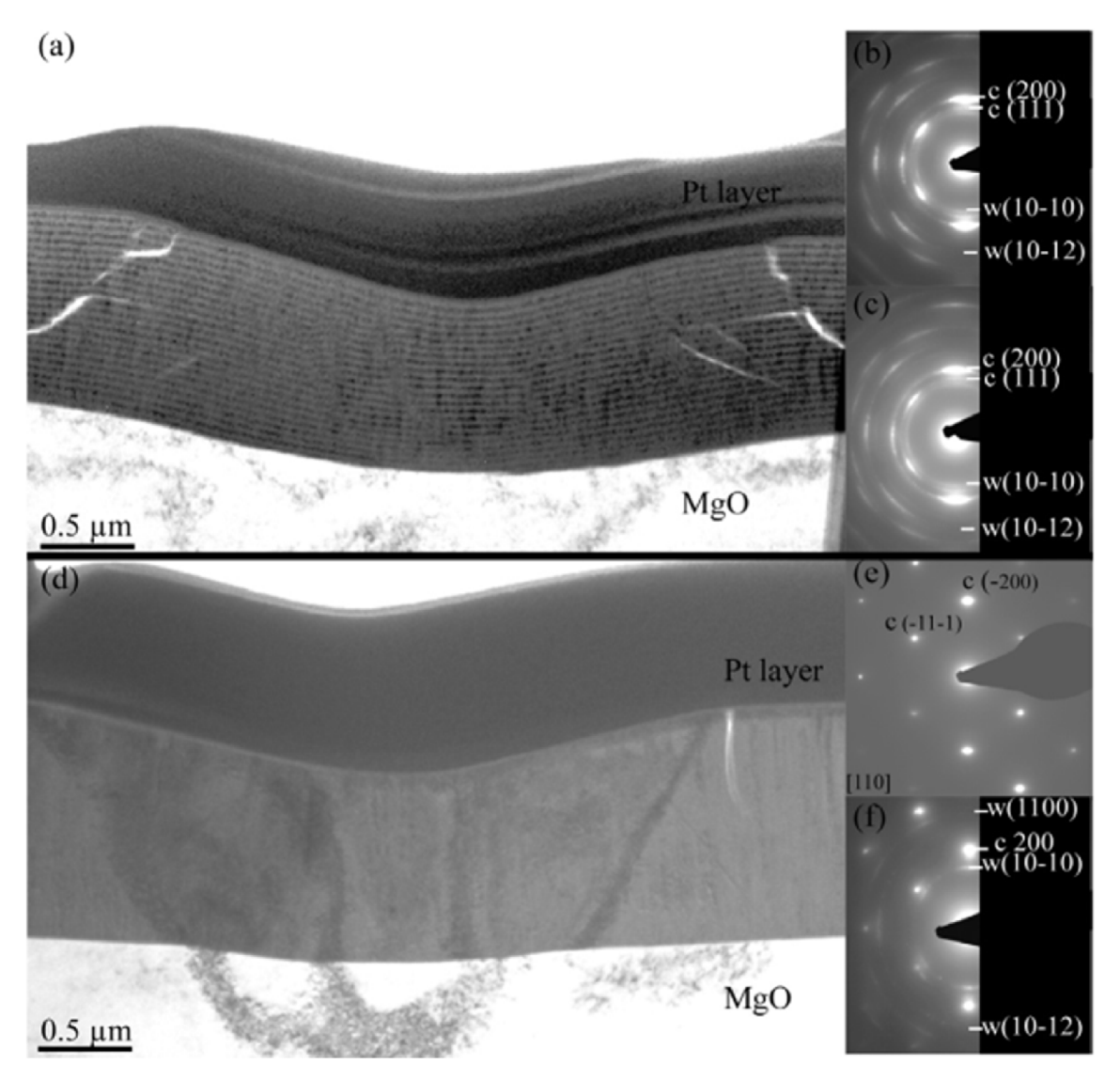


Fig. 8 – Cross-sectional BF-TEM micrographs and SAED patterns of the multilayers with a  $Zr_{0.63}Al_{0.37}N$  layer thickness of (a-c) 30 nm and (d-f) 2 nm. The SAED patterns are taken far away from the indents in (b) and (e) and under the indent in (c) and (f) [90].

and was inserted into the  $\alpha$ -Al $_2$ O $_3$  matrix. While the Al $_2$ O $_3$  and GAP phases were separated, their interface was semicoherent with no amorphous phase. The electron diffraction in Fig. 10(b and c) confirmed the apparent orientation of the two phases.

When two adjacent interfaces have different atomic configurations with interatomic distances greater than 25 %, the entire interface cannot be matched and is defined as incoherent. There are significant lattice differences between Fe (2.87 Å) and W (3.16 Å) [96]. Ren et al. [97] investigated the interfacial structure of the Fe/W nano-multilayered film and revealed that the thermal stability of the incoherent Fe/W interface was lower than the coherent interface. The reinforcement mechanism of the incoherent interface is complicated due to the lower interfacial shear strength and resulting dislocation accumulation.

Coherent interfaces can inhibit dislocation motion and refine grains. The crystal structure and similar lattice parameters at

the coherent interface allow the adjacent layers to have continuous slip systems. In addition, the small lattice mismatch generates higher stresses and improves the hardness of the film. Semi-coherent interfaces with high diffusivity and low deformation energy can also prevent slip transport and enhance hardness [98,99].

#### 3.4. Ductile metallic phase

The toughness phase in nano-multilayered films often refers to incorporating some phases with toughness or high plasticity on a brittle substrate. The ductile phase usually has a high plastic-deformation ability and good toughness, which can effectively absorb and disperse the external stress and reduce the stress concentration effect of the film, thus improving the shear resistance of the whole film. At the same time, the ductile phase can absorb more energy when the crack expands, limiting the crack expansion [100—102].

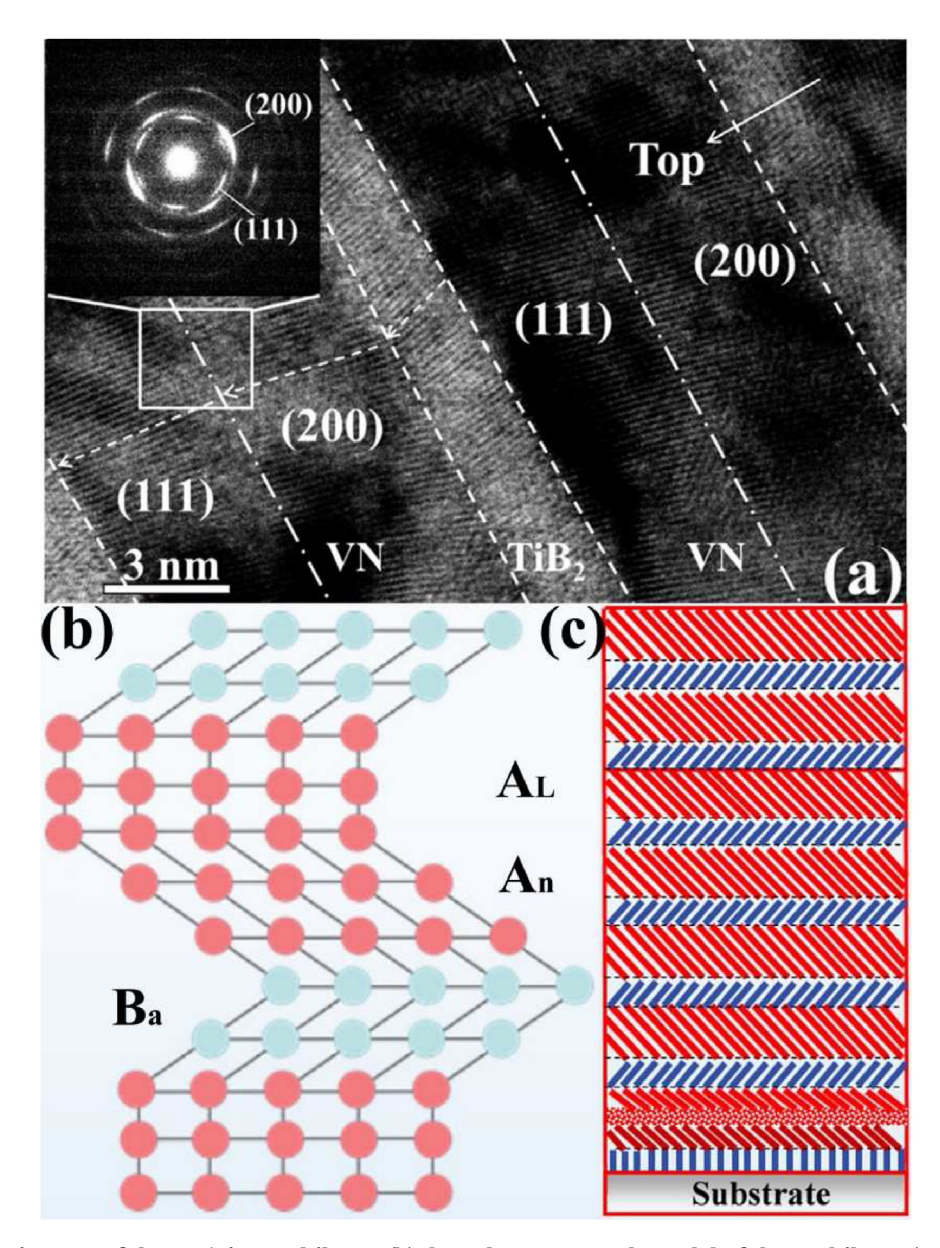


Fig. 9 – (a) HRTEM images of the VN/TiB<sub>2</sub> multilayer, (b) the coherent-growth model of the multilayer ( $A_L$ : crystal phase of minimum strain energy,  $B_a$ : epitaxial growth on  $A_L$  surface,  $A_n$ : induced to be the most stable phase to matching the  $B_a$ ) and (c) the VN/TiB<sub>2</sub> multilayer structure diagram [93].

Thinner metal layers can enhance the hardness, toughness, and wear resistance of the nano-multilayer film, and the smooth metal nanoclusters can reduce its friction coefficient. Ren et al. [39] prepared Ag/TaC nano-multilayered films with Ag thicknesses from 2 to 14 nm by magnetron sputtering. When the Ag layer was 2 nm, it formed a discontinuous growth layer that increased the film hardness to 42 GPa based on the Orowan mechanism. The nanoclusters and AgTaO<sub>3</sub> phase generated at the contact surface reduced the friction coefficient to 0.227. The (CrN/ZrN)/(Cr/Zr) nano-multilayered films contained metal modulation layers [103]. Its hardness reached 34 GPa while its H/E > 0.1 and  $H^3/E^2 = 0.36$  GPa.

The selection of appropriate materials as the ductile phase is crucial to improving the mechanical properties of nano-multilayered films. Metal is a material with good plasticity and ductility, which can be effectively used as the ductile phase in the films. The deformation of the metallic phase can absorb stresses and avoid the extension of interlayer cracks through a dislocation-slip mechanism. The Ag, Ti, and Ta cubic phase sublayers in nano-multilayered films usually exhibit better ductility and absorb considerable fracture energy during crack propagation, allowing the films to achieve excellent fracture toughness. However, HCP phases, such as W and Zr, which possess fewer slip systems, make the films exhibit strong brittle properties [3]. In conclusion, the ductile phase is an essential structure in nano-multilayered films that can significantly improve the films' toughness, ductility, and fracture resistance, enabling them to better adapt to stresses and deformations under various external environments.

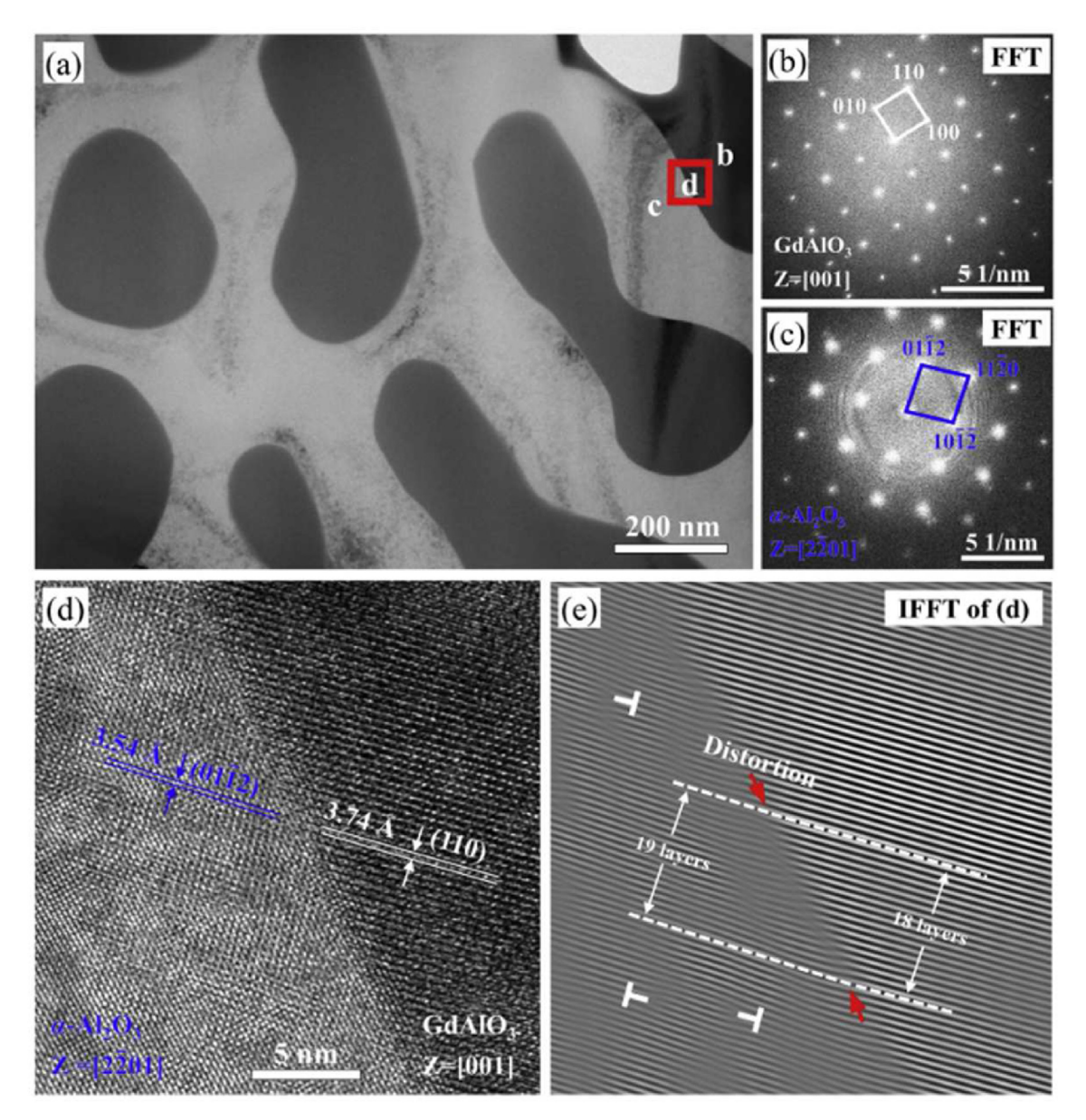


Fig. 10 – (a) bright-field TEM of the  $Al_2O_3/GAP$  rod-like eutectic in the transverse cross-section, (b and c) indexed Fast Fourier transforms, and (d) HRTEM micrograph of the interface structure along with (e) a corresponding Fourier filtered image. The red box highlights the position observed in (d) and (e) in (a) [95].

# 4. Mechanical property

#### 4.1. Hardness

Nano-multilayered films exhibit the phenomenon of superhardness when the sublayers are reduced to the nanoscale, with hardness exceeding 40 GPa [104,105]. This effect is due to the combination of their unique structures and compositions. Firstly, nano-multilayered films typically consist of interlocking nanograin layers with dense grain boundaries, which effectively restrict the grain movement and increase the hardness of the material. Secondly, by the alternate deposition, complex structures can be formed, leading to changes in the microstructures and physical properties of the material,

which ultimately contribute to the improvement of hardness. Therefore, the mechanism of super-hardness of nanomultilayered films involves a variety of factors, including the grain-boundary confinement, microstructures and compositions.

Helmersson et al. discovered the super-hardness effect in the TiN/VN nano-multilayered film with a hardness exceeding 50 GPa, which highlighted the film's significant research value and potential applications [108]. Fig. 11(a)and(b) shows the TiN/WN SL structures with a bilayer period of 8.1 nm, and the film reaches a maximum hardness of 36.7 GPa. It seems reasonable that the TiN/WN SL structures roughly follow a model that neglects coherency strains and centers on differences in the elastic moduli of the layers [106]. With experimental research and theoretical simulation, Chen et al.

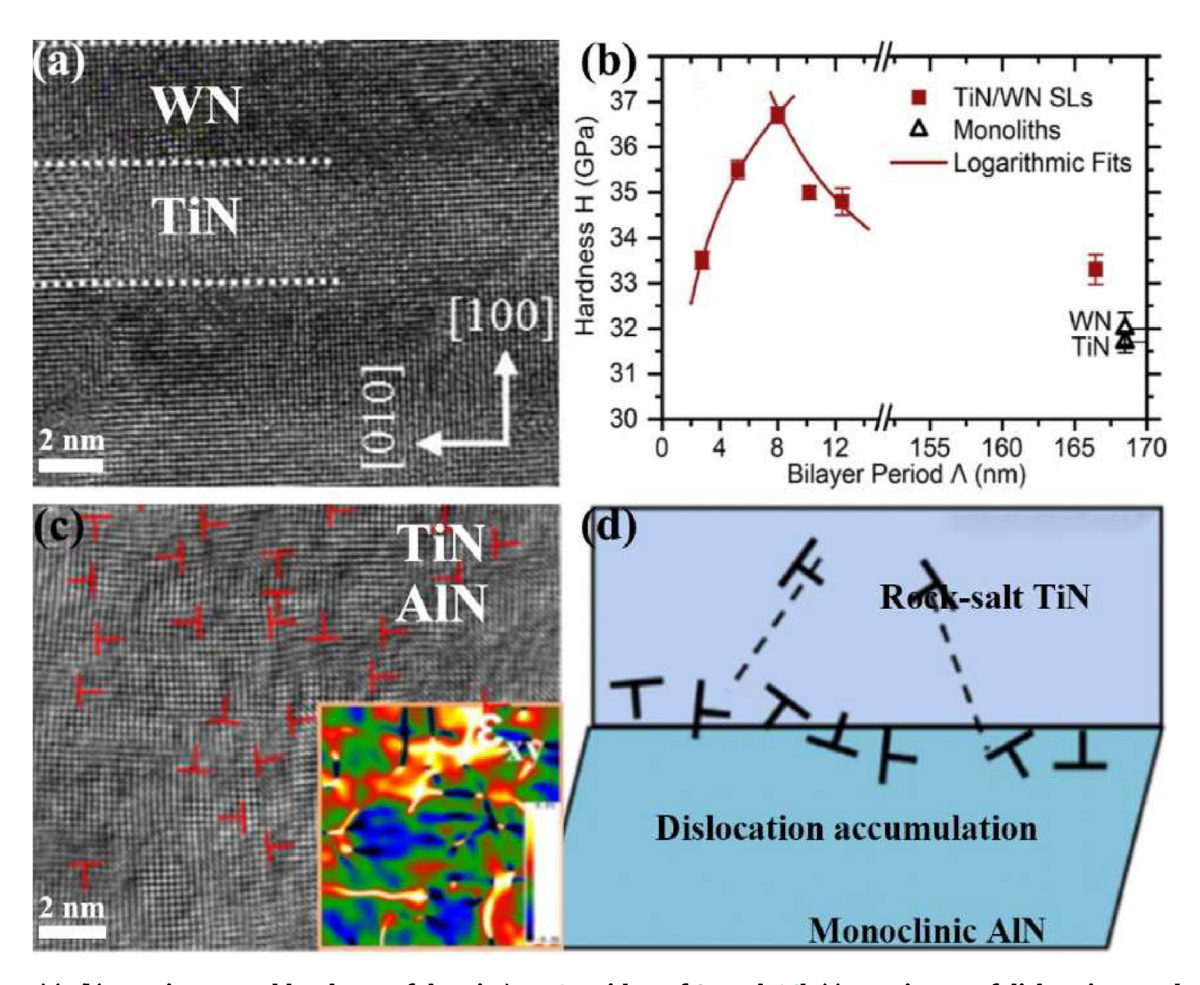


Fig. 11 - (a)–(b) TEM image and hardness of the TiN/WN SL with  $\Lambda$  of 8 nm [106]. (c) TEM image of dislocations and strain field in the deformed interface region of single-crystal TiN/AlN SL, (d) schematic of dislocation distribution in the distorted interface [107].

revealed the structural evolution of single-crystal TiN/AlN SL during nanoindentation on the atomic scale [107]. Fig. 11 (c) shows the TEM image and stress state of the interfacial deformation region of the coating. Many accumulated dislocations exist in the interfacial deformation region, as shown schematically in Fig. 11 (d). The elevated dislocation density and localized stress enhancement mainly originate from the localized phase transition within the AlN layer, leading to a high degree of lattice mismatch. Meanwhile, a smaller modulation period in the nano-multilayered film can provide more interfaces, offering enhanced strengthening properties. Ljungcrantz [109] investigated the relationship between the super-hardness effect in TiN/NbN nano-multilayered films and the  $\Lambda$ . The results revealed that when the  $\Lambda$  was 4.8 nm, the film exhibited the highest hardness of 40 GPa, significantly greater than that of TiN (22 GPa) and NbN (18 GPa). VC/AlN nano-multilayered films with an AlN layer thickness of less than 1 nm exhibit coherent growth and attain a considerably enhanced hardness of up to 40.1 GPa [110]. The CrN/MoN nano-multilayered films exhibit a high hardness of 38-42 GPa when the bilayer thickness,  $\Lambda$ , is 5.8 nm [111].

The mechanical behavior of nanofilms is influenced by several factors, including the material composition,  $\Lambda$ , interfacial structure, residual stress, dislocation slip, etc. [85,112]. Usually, the hardness of nano-multilayered films is higher

than their monolithic films or the mixing rules. The hardness is greater than 40 GPa as super-hard films [113,114]. Using the Oliver and Pharr method [115], the hardness and modulus have been computed from the indentation load-displacement data for various peak loads. The modulus, *Er*, and hardness, *H*, can be written as

$$E_{r} = \frac{\sqrt{\pi}}{2} \cdot \frac{S}{\sqrt{A}},\tag{1}$$

$$H = \frac{P_{max}}{A},\tag{2}$$

where A is the projected area of the contact at the peak load, S is the measured stiffness,

$$P = A(h - h_f)^m, (3)$$

$$h_{s} = \epsilon \frac{P_{max}}{S},\tag{4}$$

where h is the total displacement,  $h_f$  is displacement of the surface profile after load removal,  $h_s$  is the displacement of the surface at the perimeter of the contact, for the flat punch,  $\epsilon = 1$ , and the paraboloid of revolution,  $\epsilon = 0.75$ .

When the MoN sublayer thickness was 1.0 nm, the superhardness of the NbN/MoN nano-multilayered film was 40.0 GPa [105]. As the  $\varLambda$  decreased to 20 nm, the CrN/MoN nano-multilayered film hardness and H/E increased to 42.3 GPa and 0.11, respectively [116]. When the  $\varLambda$  was 4.8 nm, the hardness of the TiN/NbN nano-multilayered film was 40 GPa, and their monolithic films were 22 GPa and 18 GPa [109]. With the help of the experimental tests and first-principles calculations, it was found that the interfacial structure is the primary influencing factor for the superhardness. At  $t_{\rm SiG}=0.8$  nm, the TaC/SiG nano-multilayered film formed excellent coherent interfaces with the hardness and toughness reaching 46.1 GPa and 4.21 MPa m<sup>1/2</sup>, respectively [117].

Table 2 presents the super-hardness values, preparation parameters, and structural characteristics of the nanomultilayered films. Typically, the increase in hardness is attributed to the difference in the shear modulus between the two modulated layers and the restricted movement of dislocations at the interlayer interface. These mechanisms will be thoroughly discussed in Section 5.2 hardness enhancement mechanism.

#### 4.2. Toughness

With the degradation of the service environment, the importance of film toughness alongside hardness has gained recognition. To assess the fracture toughness of coatings, proxies such as H/E and  $H^3/E^2$  (where H represents hardness and E represents elastic modulus) have been proposed. A higher value of H/E or  $H^3/E^2$  indicates reduced plastic deformation under stress, thus indicating greater toughness [31,122]. One possible rationale for using H/E as a proxy for fracture toughness is that H is directly related to the yield strength  $(\sigma_y)$ , making H/E a measure of the elastic-strain limit, which is often interpreted as toughness. Additionally, Greenwood and Williamson's work may have contributed to this perspective by defining the plasticity index,  $\varphi$ , as follows [123]:

$$\varphi = \frac{E}{H} \left(\frac{\sigma}{\beta}\right)^{\frac{1}{2}} \tag{5}$$

where  $\sigma$  is the surface roughness, and  $\beta$  is the asperity radius. H/E is inversely proportional to the plasticity index at the constant surface roughness and asperity radius. Therefore, it can be argued that a coating with a higher H/E value is less prone to plastic deformation under a given stress, indicating higher toughness in scenarios without plastic deformation.

The adoption of the  $\rm H^3/E^2$  likely originated from the analysis of sphere-on-flat Hertzian contact [124]. In this analysis, a contact is established between a sphere with a radius, R, and an elastic modulus, E, and an infinitely rigid flat surface subjected to an average load, N. The maximum Hertzian contact stress,  $\rm P_{max}$ , is given by the equation:

$$P_{max} = \frac{1}{\pi} \left( \frac{6NE^2}{R^2} \right)^{\frac{1}{3}} \approx 0.578 \left( \frac{NE^2}{R^2} \right)^{\frac{1}{3}}$$
 (6)

Significant plastic deformation is absent when  $P_{\rm max} < \sigma_y$ , which is assumed to be proportional to the coating hardness, H, resulting in the inequality,

Table 2 – Hardness values of several nano-multilayered fil	of several nano-multilay	ered films measured via nanoindentation.	oindentation.		
Composition	Technology	Parameter	Characteristic	H (GPa)	References
Ti(CuNiZr)N/AlCr(SiW)N	arc ion plating	I	1	36.0	[1]
$VN/TiB_2$	magnetron sputtering	t <sub>VN</sub> :t <sub>TiB2</sub> to 1:7	coherent growth	41.8	[63]
NbN/MoN	magnetron sputtering	MoN 1.0 nm	narrow interface, block the movement of dislocations	40.0	[105]
CrN/MoN	arc ion plating	1	increase interface, prevent dislocation movements,	42.3	[111,116]
TaC/SiC	magnetron sputtering	$t_{SiC} \leq 0.8 \ nm$	SiC crystallized and grew coherently with TaC	46.1	[117]
TiSiN/Cu	arc ion plating	copper 97.10 nm	columnar broken, copper diffusion, solid solution hardening	40.4	[118]
Tin/Alon	magnetron sputtering	AlON less than 0.6 nm	crystallize and grow epitaxially	40.5	[119]
VC/SiC	magnetron sputtering	SiC below 0.7 nm	crystallized, grew coherently	36.1	[120]
AlCrN/TiSiN	magnetron sputtering	bias voltage 50 V-110 V	(200) to (200) and (111) FCC, epitaxial growth, lattice misfit	36.5	[121]

$$0.578 \left(\frac{NE^2}{R^2}\right)^{\frac{1}{3}} < \sigma_y = \alpha H \tag{7}$$

where  $\alpha$  is some constant, therefore, one can write:

$$N < 5.168\alpha^3 R^2 \frac{H^3}{F^2} \tag{8}$$

The above equation signifies that, for a given external load and test geometry, a coating with a higher  $H^3/E^2$  value is less likely to experience plastic deformation and is therefore expected to possess greater toughness [122].

In addition, the fracture toughness of the nano-multilayered films can be further evaluated by the following equation [125]:

$$K_{IC} = \delta \left(\frac{E}{H}\right)^{\frac{1}{2}} \left(\frac{P}{c^{\frac{3}{2}}}\right),\tag{9}$$

 $K_{IC}$  is the critical stress intensity of factor. which describes the ability of the material to resist fracture [126,127].  $\delta$  is the Berkovich type, c ( $\mu$ m) is the average value of the radial crack lengths. P (mN) is the maximal load. H and E are hardness and modulus values.

Ou et al. prepared CrN/Si<sub>3</sub>N<sub>4</sub> nano-multilayered films with 1.1-25.1 at.% Si [41]. When the Si content was 15.2 at.%, the microstructure showed dense fibrous grains, and the films' H/ E,  $H^3/E^2$ , and  $K_{IC}$  values reached 0.099, 0.387 GPa, and 3.69 MPa  $\mathrm{m}^{1/2}$ , respectively. Liu et al. fabricated TiAlN/CN $_{\mathrm{x}}$ nano-multilayered films with the same thickness of both modulated layers and sublayer thicknesses ranging from 0.9 nm to 13.7 nm [76]. When the TiAlN sublayer thickness was 0.9 nm, the CN<sub>x</sub> sublayer was inserted into the TiAlN grains to form a nanocomposite structure. At the TiAlN sublayer thickness of 2.6 nm, the CN<sub>x</sub> sublayer grew in coherent epitaxy with the TiAlN sublayer. The fracture toughness of the nanomultilavered films was enhanced by 1.5 times. The TiN/WN nano-multilayered films obtained a maximum fracture toughness of 4.6  $\pm$  0.2 MPa m<sup>1/2</sup> at a bilayer period of 10.2 nm, which is larger than the  $2.8 \pm 0.1$  and  $3.1 \pm 0.1$  MPa m<sup>1/2</sup> values for monolithic TiN and WN, respectively [106]. Table 3 lists the results of toughness evaluations by K<sub>IC</sub>, H/E, and H<sup>3</sup>/E<sup>2</sup> for some nano-multilayer films. The fracture toughness of the nano-multilayered films significantly depends on the preparation method, modulation period, modulation ratio, and material composition.

#### 4.3. Tribological behavior and wear resistance

Nano-multilayered films have several advantages over other coatings, such as high hardness and modulus, good densities, and low residual stresses, significantly improving their friction and wear resistance. The higher hardness of nano-multilayered films allows them to withstand the impact of external physical and chemical factors. For instance, they can maintain stable surface properties even under elevated temperatures, high pressure, or intense acidic and alkaline environments. The multilayer structure of nano-multilayered films provides additional protection by relying on other layers, even if one of the layers is subjected to wear or scratches. The multilayer structure also increases the elasticity and toughness of the film layers, thus improving their resistance to wear and tear [82,94,100,132].

The MoN $_x$ /SiN $_x$  nano-multilayered films were prepared by magnetron sputtering [133]. The friction coefficient decreased to 0.53 when the microstructure transformed from the amorphous to crystalline phase. The CrN monolithic film and Cr/CrN nano-multilayered film were deposited on AISI 304 SS, and the friction coefficient decreased from 0.61 to 0.46 [134]. The MoS $_2$ /Zr nano-multilayered films with different Zr doping were prepared by magnetron sputtering [38]. The optimized Zr doping and unique nanostructure resulted in a low friction coefficient of 0.05. The TiB $_2$ /Cr nano-multilayered films were fabricated by magnetron sputtering [135]. The plastic deformation of the Cr sublayer and the friction generated B $_2$ O $_3$  combined to reduce the friction coefficient of the films to 0.48 with a wear rate of  $10.1 \times 10^{-5}$  mm $_3$ /N m.

Table 4 shows the tribological test structures of some nano-multilayered films and their preparation methods. Overall, hard nano-multilayered films have excellent friction and wear resistance due to their great hardness, low coefficient of friction, and good lubrication properties, and they are widely used in practical applications.

Composition	Technology	$K_{IC}$ (MPa·m <sup>1/2</sup> )	H/E	H <sup>3/</sup> E <sup>2</sup> (GPa)	References
a-CuZr/c-ZrN	magnetron sputtering	0.5468	_	_	[22]
TiAlN/Zr <sub>3</sub> N <sub>4</sub>	magnetron sputtering	_	0.14	_	[25]
AlCrN/AlCrSiN	arc ion plating	9.8	0.10	0.29	[26]
Ti/TiN	magnetron sputtering	+82 %	-	-	[36]
AlCrN/Cu	arc ion plating/magnetron sputtering	_	0.08	_	[37]
CrN/Si <sub>3</sub> N <sub>4</sub>	magnetron sputtering	3.69	0.10	0.39	[41]
Ti/TiN	arc ion plating	_	0.07	0.11	[43]
Ti(CuNiZr)N/AlCr(SiW)N	arc ion plating	_	0.09	0.29	[1]
CrAlN/CrN	arc ion plating	10.3	_	-	[73]
Ti/TiAlN	arc ion plating	_	0.08	0.22	[74]
TiAlN/CN <sub>x</sub>	magnetron sputtering	1.5 times	0.08	0.18	[76]
TaC/SiC	magnetron sputtering	4.21	_	-	[117]
multilayer diamond-like carbon	magnetron sputtering	_	0.10	0.12	[128]
MoS <sub>2</sub> /WS <sub>2</sub>	magnetron sputtering	-	0.09	0.05	[129]
AlTiN/AlCrSiN	arc ion plating	_	0.07	_	[130]
CrAlN/TiSiN	magnetron sputtering	_	twice	_	[131]

Composition	Technology	Tribological behavior		References
		COF	wear rate (mm <sup>-3</sup> ·Nm <sup>-1</sup> )	
AlCrN/AlCrSiN	arc ion plating	0.54	$4.2*10^{-7}$	[26]
AlCrN/Cu	arc ion plating/magnetron sputtering	0.39	_	[37]
MoS <sub>2</sub> /Zr	magnetron sputtering	0.05	_	[38]
CrN/Si <sub>3</sub> N <sub>4</sub>	magnetron sputtering	0.45	$1.3*10^{-7}$	[41]
Γi/TiN	arc ion plating	0.28	_	[43]
Cr/CrN	arc ion plating	0.28	_	[59]
Ni-Co-P	electrodeposition	0.40	_	[70]
MoN/TiSiN	arc ion plating	0.32	_	[75]
ΓiAlN/AlN	magnetron sputtering	0.61	_	[77]
ΓiMoN/Si <sub>3</sub> N <sub>4</sub>	magnetron sputtering	0.55	_	[78]
AlTiSiN/AlCrSiN	arc ion plating	0.26	_	[87]
NbN/MoN	magnetron sputtering	0.53	_	[105]
AlTiN/AlCrSiN	arc ion plating	lowest	$1.1*10^{-6}$	[130]
CrAlN/TiSiN	magnetron sputtering	four times lower	lower wear	[131]
MoN <sub>x</sub> /SiN <sub>x</sub>	magnetron sputtering	0.53	_	[133]
CrN/Mo <sub>2</sub> N	arc ion plating	0.33	7*10 <sup>-7</sup>	[136]

#### 4.4. Corrosion resistance

Corrosion resistance refers to the film's ability to resist corrosion in various corrosive media. The multilayer structure of the nano-multilayered film can effectively increase the interface area and reduce the film's surface roughness, making it challenging for corrosive media to invade the film's interior. At the same time, the interface can improve the mechanical strength and hardness of the film and inhibit the occurrence of internal cracks and defects. Nano-multilayered films can resist different corrosive media by adjusting the chemical composition and thickness between different layers. Introducing lattice strains can regulate the films' corrosion resistance by influencing their structures and properties in preparing nano-multilayered films [137,138].

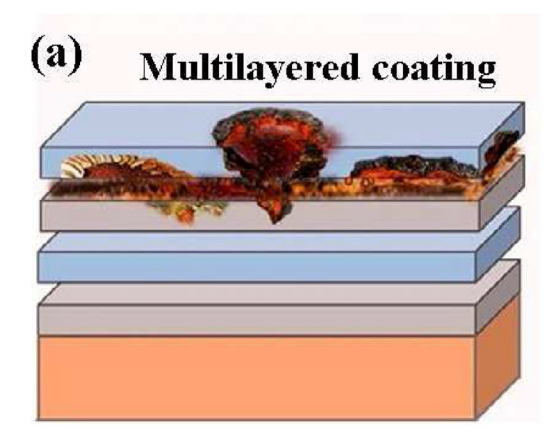
The enhanced corrosion resistance of multilayered coatings, compared to single-layer coatings, is attributed to the formation of new interfaces, which allow the lateral diffusion of the corrosive medium rather than the direct penetration into the substrate. In Fig. 12 (a), the lateral diffusion of the corrosion medium causes a lag in the corrosion rate of the multilayered coating, while in the homogeneous coating, the corrosion medium can directly penetrate into the substrate, as shown in Fig. 12(b). The CrN, CrAlN, and CrAlN/CrN multilayer coatings were deposited on Ti6Al4V substrates, employing a multi-arc ion-plating technique by Guo et al. [73]. The results showed that the best corrosion resistance of CrAlN/CrN coatings was 0.03 mg cm<sup>-2</sup>·min<sup>-1</sup> and 0.10 mg cm<sup>-2</sup>·min<sup>-1</sup> when the impact angles were 30° and 90°, respectively. The interface in the films effectively inhibited crack expansion and improved the corrosion resistance of the coating. The CrN/ CrAlN nano-multilayered films were deposited on 316L SS [140], which had lower interfacial contact-resistance values than those of CrN and CrAlN films. The maximum power density was 0.93 W/cm<sup>2</sup> at 2 A/cm<sup>2</sup> and the output voltage of 0.96 V. The MoS<sub>2</sub>/WS<sub>2</sub> nano-multilayered film was prepared by magnetron sputtering [129]. Its dense microstructure and multilayer interface impede the corrosion diffusion of H<sub>2</sub>O, O<sub>2</sub>, Cl<sup>-</sup>, and Na<sup>+</sup>, significantly improving the films' corrosion resistance. The Ti/TiN nano-multilayered films were prepared

by multi-arc ion plating on a Ti6Al4V alloy [43]. The Ti sublayer can refine the grains and prevent crack initiation and expansion. Compared to the Ti6Al4V alloy and TiN films, the corrosion resistance of the nano-multilayered film was improved by 58 times and 2 times, respectively. The TiN/AlN nano-multilayered films with  $\varLambda$  from 2 to 12 nm were prepared by magnetron sputtering [89]. When  $\varLambda=12$  nm, the modulation layer of the nano-multilayered films exhibited a coherent epitaxial structure, which hindered the diffusion of the corrosive liquid and electrochemical decomposition. The better fracture toughness, dense microstructures, and coherent interfaces have more crucial effects on the erosion resistance of the nano-multilayered films.

#### 4.5. Oxidation resistance and thermal stability

Nano-multilayered films resist oxygen-atom diffusion and can maintain their structural integrity and properties in hightemperature environments. They can also be utilized for preparing high-temperature stable thermal barrier coatings [34,141-143]. The nanometer-thick multilayer structure causes oxygen molecules to undergo multiple reflections and scattering when passing through the film layers, reducing their contact time and probability with the substrate surface, which decreases oxidation reactions. Additionally, the interfacial regions between the nano-layers offer physical protection by effectively isolating the material from external substances, such as oxygen and water vapor. The nanomultilayered film's uncoordinated atoms and structural defects can absorb oxygen molecules, undergo their redox reactions, and convert oxygen into more stable oxides, thus preventing further oxidation reactions [58,140,144,145].

Liu et al. [146] fabricated a Cr–CrN/TiSiN–Cr nanomultilayered films on Zircaloy. During oxidation at 1200 °C for 25 min, Zr in the substrate and Si in the film diffused to the surface, forming  $\rm ZrO_2$  and  $\rm SiO_2$  protective layers, respectively, and the film effectively protected the substrate from oxidation. The AlN/CrN nano-multilayered film was deposited on AISI 316 by magnetron sputtering [147]. During oxidation at 900 °C for 60 min, Cr diffused along the grain boundaries to the



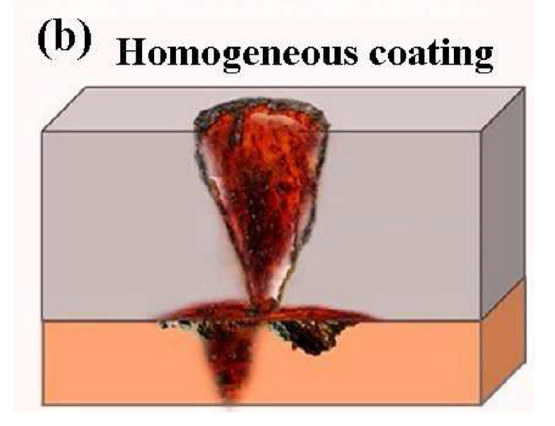


Fig. 12 — Schematic of the corrosion mechanism in multilayer and monolayer alloy coatings [139]. (a) Spreading of corrosive agents laterally through new interfaces, (b) Penetration of the corrosive agent directly to the substrate.

surface, forming  $\rm Cr_2O_3$  and the columnar grains at the coherent interface, resulting in the film exhibiting oxidation resistance. Wang et al. [141] prepared AlCrSiN/VN nanomultilayered films using a hybrid deposition system combining arc-ion plating and pulsed DC magnetron sputtering. The AlCrSiN sublayer effectively prevented the outward diffusion of V elements to the surface of the AlCrSiN/VN films at high temperatures, improving the oxidation resistance of the coating and delaying the initial oxidation temperature to 450 °C. The isothermal oxidation of AlCrSiN/VN films at 600 °C indicated the outward diffusion of V and Al to form  $\rm V_2O_5$  and AlVO<sub>4</sub> phases. At annealing temperatures of 800 °C to 1000 °C, the V(Cr)—N bond decomposes, and the V<sub>2</sub>N phase appears at 1100 °C.

Table 5 presents the oxidation resistance and thermal stability properties of various nano-multilayered films. These outstanding properties can be optimized by selecting appropriate materials, film structures, and preparation methods for specific applications. Generally, metallic materials, such as copper, aluminum, and molybdenum with high melting points and excellent oxidation resistance properties, are chosen for nano-multilayered films. Secondly, adjusting the nano-multilayered film structures, such as increasing the number of layers, altering the layer thickness, and designing the interleaved structure, can enhance the film's properties. Finally, appropriate preparation-process parameters are selected to obtain high film densities and crystallinity. As

a result, the oxidation resistance and thermal stability of nano-multilayered films can be improved.

#### 5. Future research directions

#### 5.1. New nano-multilayered film types

High entropy alloy films are a new material consisting of multiple elements with relatively balanced contents, exhibiting prominent high-entropy characteristics. They possess higher hardness and strength, good toughness and plasticity, and better chemical stability and corrosion resistance [2,152]. Using high-entropy ceramic films as the modulation layer can improve the crystal structure of the nano-multilayered film. The similar thermal expansion coefficients among the elements of high-entropy alloys can form good interfacial bonding and improve the interfacial bonding between different materials in multilayer films [153–155]. Therefore, introducing high-entropy-alloy modulation layers is essential for enhancing the performance of nano-multilayered films.

Based on the above analysis of nano-multilayered film types, researchers hope to develop more types of nano-multilayered films, such as Ti/TiN/Zr/ZrN [156], Ti-DLC [157], TiSiN/Ag/TiSiN [158], (CrN/ZrN)/(Cr/Zr) [103], (AlCrTiZrNb)N/WS $_2$  [153], nano-multilayered films with nanocomposite films as modulation layers, high-entropy alloy-based nano-

Composition	Technology	T (°C)	References
AlCrN/Cu	arc ion plating/magnetron sputtering	800	[37]
$(Al,Cr)_2O_3/ZrO_2$	arc ion plating	1100	[58]
AlTiN/AlCrSiN	arc ion plating	800	[130]
Zr/Nb	magnetron sputtering	350	[148]
Cu/W	magnetron sputtering	700	[149]
SiO <sub>2</sub> /NbSi <sub>2</sub>	halide-activate pack cementation	1250	[143]
TiB <sub>2</sub> /Cr	(high power impulse + direct current) magnetron sputtering	500-600	[132]
CrCN/TiSiCN	arc ion plating + magnetron sputtering	1000	[144]
CrAlN/SiN <sub>x</sub>	magnetron sputtering	1000	[150]
Ni/Ni <sub>3</sub> Al-W	magnetron sputtering	800	[151]

multilayered films, and other high-quality nano-multilayered films. Fig. 13 shows a novel (diamond/β-SiC)/microcrystalline diamond (MCD) multilayer with nanocrystalline diamond (NCD) top layer structure on a cemented carbide substrate [159]. The experimental results indicated that the multilayer coating achieved an ultra-hardness of 83.6 GPa and had a low residual stress of -1.2 GPa, excellent adhesion (52.9 N), and resistance to crack expansion. In this coating, the MCD layer ensured the hardness and elastic modulus, and the diamond/ β-silicon carbide composite layer had better bonding properties and lower residual stresses. Which provided a new way to develop high-performance nano-multilayered films. Penkov et al. developed SiN<sub>x</sub>/BN periodic multilayered coatings [160]. The coating thickness of 150 nm could achieve a hardness of 35 GPa. The reflectivity of the coating was 8 % in the visible light range. The coating showed high wear protection, and no significant cracks or delamination were observed after 1000 cycles of sliding silicon nitride balls on the surface.

#### 5.2. Hardness enhancement mechanisms

The strengthening mechanisms of nano-multilayered films has been extensively discussed and demonstrated for decades. The effectiveness of the mechanical-property enhancement of nano-multilayered films is closely related to the film material, modulation cycle, and other preparation processes, such as pressure and power. The strengthening mechanism of the nano-multilayered film is explained by several theories, including the Koehler model [15], the Hall-Petch relationship [161], and the theory of alternating stress field effects [162].

Koehler [15] proposed the modulus differencereinforcement theory, which suggests that dislocations experience a mirror force at the coherent interface as they cross it within the nano-multilayered films. This force arises from the presence of dislocations with varying linear energies in layers characterized by different shear moduli. When dislocations cross from a low shear-modulus layer to a high shear-modulus layer, they require an additional stress, hindering their motion and strengthening the nano-multilayered films. The reinforcement effect becomes more pronounced as the difference in shear modulus between the two layers increases. The hardness increment ( $\Delta H$ ) can be mathematically expressed as follows [163]:

$$\frac{3(1-\nu)(G_{\text{A}}-G_{\text{B}})\sin\theta}{m\pi^2} \leq \Delta H \leq \frac{3(G_{\text{A}}-G_{\text{B}})\sin\theta}{m\pi^2}, \tag{10}$$

where G is the shear modulus,  $\nu$  is the Poisson ratio,  $\theta$  represents the angle between the slip surface of the low modulus layer and the coherent interface [163]; m corresponds to the Taylor factor, and the nitride ceramic phase can take 0.3 [164].

To elucidate the phenomenon of hardness enhancement in nano-multilayered films, Kato introduced the alternating stress-field theory [165]. The results suggest that the nano-multilayered films' coherent interfacial stress field may strengthen them. During the growth of nano-multilayer films, coherent growth occurs between layers due to the small modulation thickness of the modulation layer. At this time, the modulating layer with a smaller lattice constant is subjected to a tensile stress caused by the adjacent modulating layer. In comparison, the modulating layer with a larger lattice constant is subjected to a compressive stress caused by the adjacent modulating layer, which produces an alternating tension and compression stress field in the film. The corresponding increase in the film hardness ( $\Delta H$ ) can be expressed as follows [165]:

$$\Delta H \cong 3\sigma = \frac{\sqrt{6}}{2} A \epsilon E_{ave}, \tag{11}$$

The modulation amplitude, A, is connected to the modulation period and the degree of interfacial mixing in the film, which takes 0.5 [166],  $\varepsilon$  is the lattice mismatch between the two layers of the material, E corresponds to the average elastic moduli of the two layers of the materials.

In metallic materials, the Hall-Petch theory is a classical theory that expresses the relationship between the yield

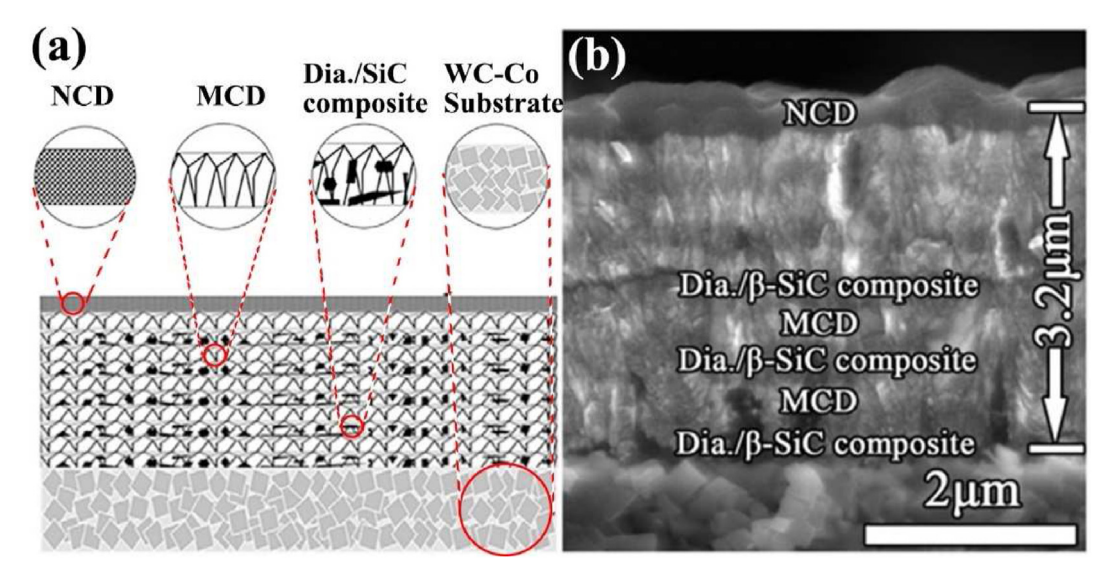


Fig. 13 — Cross-sectional morphologies of the (Diamond/ $\beta$ -SiC composite)/MCD multilayer + NCD top layer coating: (a) illustration of the architectures model microcrystalline coating, (b) cross-sectional SEM morphologies of the coating [159].

stress and grain size of materials [167]. According to this theory, the mechanical properties of metallic materials are strengthened by refined grains as the grain size decreases. The theory can be expressed as follows:

$$\sigma_{\rm c} = \sigma_0 + K_{\rm H} D^{-1/2},$$
 (12)

where  $\sigma_c$  is the material's yield stress at a grain size, D,  $\sigma_0$  is the yield strength of the material in the bulk state,  $K_H$  is the calculated constant of the hardness and grain-boundary dependence, and D is the average grain size of the material.

The mechanism of generation, failure, reversal, and gradual smoothing of the Hall-Petch effect in nanoceramic materials is not exactly the traditional simple diffusion effect [168]. The changes in the mechanical properties, density, and dissipation energy are directly related to the grain-boundary volume. The hardness and strength of ceramic materials in a specific size range will also increase with the grain-size reduction, resulting in fine-grain strengthening. In addition, Lu et al. investigated the influence of interfacial structure on the super-hardness effect of TiN (111)/NbN(111) nanomultilayered film by first principles [169]. The results show that the N-Nb termination structure and interface configuration break the continuous NaCl structure of TiN, which is the dominant factor affecting the super-hardness effect, The bonding behavior of the interface is the second factor. Compared with the interface's ionic character, the covalent character's hardness can be neglected.

#### 5.3. Toughening mechanism

Toughening nano-multilayered films involves introducing structural defects or features to improve their toughness and strength [170–173]. The toughening mechanism of nano-multilayered films includes the deflection of cracks,

hindrance of crack extension, crack coupling, nano-plasticity, and stress-concentration release, as shown in Fig. 14 (a) [174].

Adding alloying elements at sub-layers can increase the plasticity of the film, reducing the stress concentration and improving toughness and strength. As shown in Fig. 14(b) and(c), more interface cracks bridging and crack deflection are noticed when the Y/VO2 ratio of the ZrOxNv/V2O3-Y nanomultilayered is 5/10. It is attributed to incorporating Y atoms to make the interface coherent, effectively improving fracture toughness [175]. The alternating layer structure impedes crack propagation, forcing cracks to shift the direction and consume more energy, making it useful for applications requiring resistance to tensile or bending stresses. In Fig. 14(d) and (e), few lateral cracks and delamination are observed in the Ti/ TiAlN multilayer coating compared to the TiAlN monolithic coating. It is because the former has many strong interfaces, and the ductile Ti layers coordinate the deformation between the TiAlN layers [176]. To investigate the role of graphene interfaces in the strengthening and toughening of Cu-graphene nanocomposites, Lee et al. [177] compared experimental and molecular dynamics (MD) simulations in Fig. 14(f)-(h). TEM revealed that dislocation motion through the graphene interface and grain boundaries was confined within individual Cu grains. MD simulations confirmed that the localized deformation resulting from the confined dislocation motion led to nucleation and growth of holes at the graphene interface, which were precursors of cracks.

The adhesion between nano-multilayered structures reduces the cracking of sublayers [171]. TiAlSiN/TiN nano-multilayered films were fabricated by multi-arc ion plating [60]. The H/E and  $\rm H^3/E^2$  were 0.072 and 0.135 GPa, respectively. The high toughness was attributed to the favorable adhesion of the nano-multilayered structure. The W/(Ti/Ta/Ti) nano-multilayered films were prepared, using the sintering

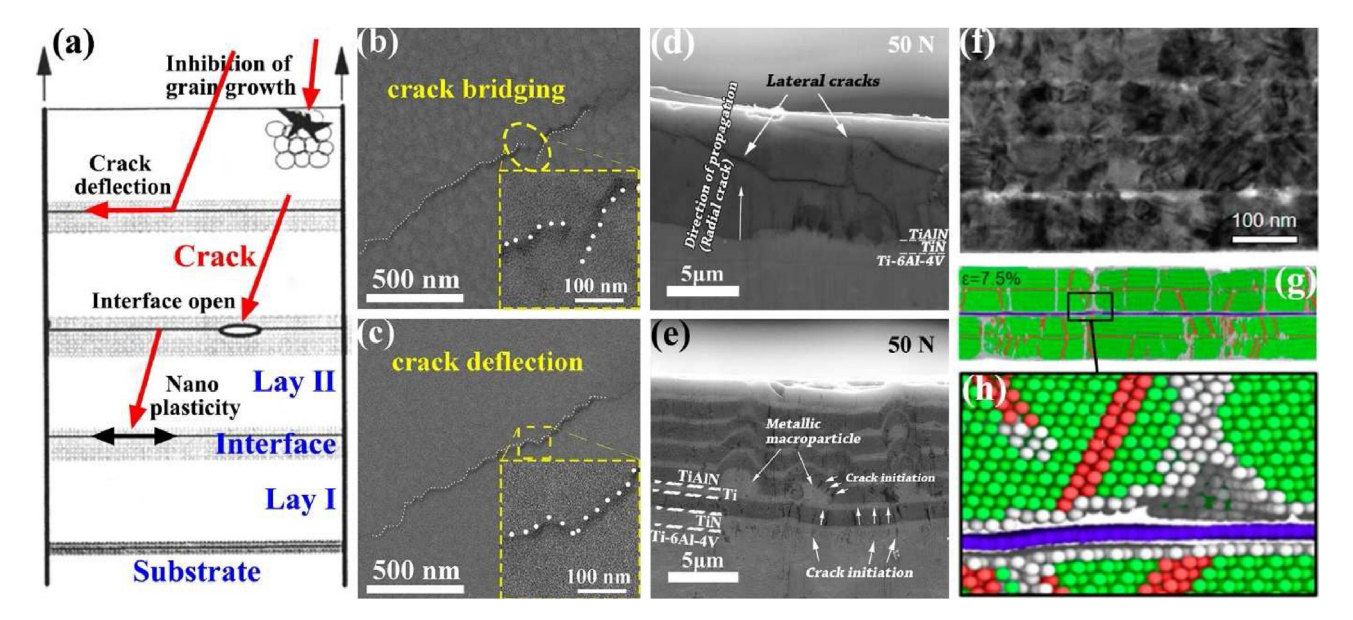


Fig. 14 – The toughening mechanism in ceramic-multilayer materials: (a) schematic diagram [174], (b)–(c) crack bridging and crack deflection in  $ZrO_xN_y/V_2O_3$ –Y nano-multilayered films [175], (d)–(e) scratch tests of TiAlN monolithic and Ti/TiAlN multilayer coatings [176], (f)–(h) HRTEM image of the graphene interface and MD simulation results of deformation evolution in Cu-Gr multilayer films [177].

technique at 1000 °C to 1400 °C [178]. Its bending strength reaches 1700 MPa at 1200 °C, which is attributed to the excellent adhesion of the microstructure. Secondly, the finer grains in the strengthening mechanism contribute to the fracture toughness of the nano-multilayered film [179]. Compared with the hardness of monolithic TiN films, the fracture toughness of the Ti/TiN nano-multilayered film was improved by 82 % because of the alternate deposition of rigid and ductile layers [36]. The TiAlN/Zr<sub>3</sub>N<sub>4</sub> nano-multilayered films were obtained by magnetron sputtering [25]. When the modulation layer, Zr<sub>3</sub>N<sub>4</sub>, was 4.2 nm, the films showed a large plastic deformation with numerous nanoscale longitudinal and transverse cracks observed in their microstructures.

Overall, nano-multilayered film toughening is complex and involves material microstructures and physical properties. Understanding these mechanisms can help design and fabricate more ductile and stronger materials for different applications. Combining techniques and approaches, such as structural-design optimization, material exploration, new preparation technologies, and computational simulations, can improve toughness and strength. Investigating the multilayer-film design, exploring materials with different lattice structures, and utilizing new preparation and processing techniques can improve toughness and strength. Computer simulations can predict and optimize nanomultilayered film properties, guiding experimental design and data analysis.

# 5.4. Nano-multilayered films with multiple excellent properties

The protective properties of conventional materials are no longer sufficient to meet the demands of harsh environments, such as high temperatures, high pressures, acids, and bases [10,82,135]. As a result, protective films with higher-performance levels have been developed to provide excellent hardness, wear resistance, and corrosion resistance. These films protect industrial equipment and materials, increase their service life, improve productivity, and enhance economic efficiency [139,148,180].

Nano-multilayered films with high hardness and toughness are manufactured by interacting multilayer structures, which effectively alleviate the conflict between the hardness and toughness. For instance, nano-multilayers can create high-strength and toughness parts and coatings in the automotive, aerospace, and mechanical fields to improve their durability and service life. Fig. 15 presents that for a shorter modulation period, K<sub>IC</sub> increases significantly, while the hardness of the nano-multilayer film also reaches a peak [181]. The consistency between K<sub>IC</sub> and hardness indicates that adjusting the nanolayer structures can enhance both the hardness and fracture toughness. By adjusting the combination and thickness of different materials, nano-multilayer films with excellent comprehensive characteristics, such as high mechanical properties, thermal stability, and oxidation resistance, can be obtained. Compared to monolithic VN and AlCrSiN, the nano-multilayered AlCrSiN/VN coating exhibited superior properties under the same preparation conditions [141]. It displayed the highest hardness of 30.7 GPa, the lowest wear rate of 2.6  $\times$  10<sup>-6</sup> mm<sup>-3</sup>·Nm<sup>-1</sup> at 600 °C, the lowest

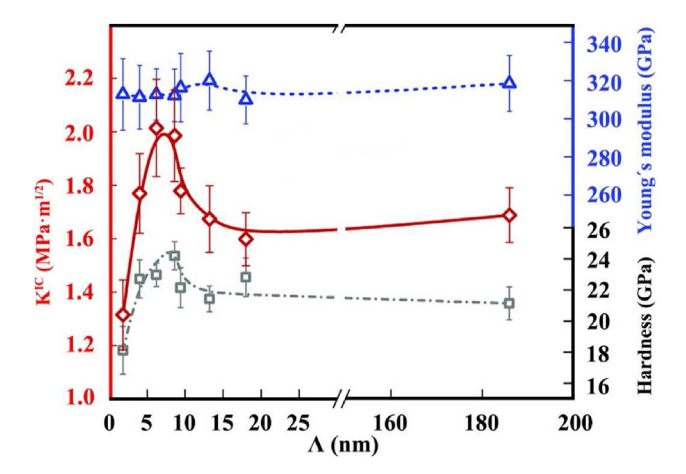


Fig. 15 – Fracture toughness,  $K_{IC}$ , indentation hardness, H, and moduli, E, of our TiN/CrN SL thin films as a function of their bilayer period,  $\Lambda$  [181].

friction coefficient of 0.26 at 800  $^{\circ}$ C, and a relatively low wear rate of 3.9  $\times$  10<sup>-5</sup> mm<sup>-3</sup>·Nm<sup>-1</sup>. Li et al. employed the magnetron-sputtering technique to fabricate Cr/CrN multilayer coatings on the Zr-4 alloy [182]. The high-temperature oxidation experiments revealed that the Cr/CrN coating displayed exceptional corrosion and oxidation resistance. Notably, a self-forming ZrO<sub>2</sub> layer with a uniform and dense thickness was observed at 1200  $^{\circ}$ C, which contributed to the durability of the Cr/CrN multilayer coating while effectively protecting the Zr-4-alloy claddings.

In summary, nano-multilayered films with high hardness, toughness, good wear-resistance, and corrosion-resistance properties have many promising applications in materials science and engineering technologies. The synergy of these properties can lead to more efficient, economical, and sustainable solutions for industrial production and daily life.

#### 5.5. Modeling and simulation

Modeling and simulating nano-multilayered films is a crucial research tool in materials science and nanotechnologies. These processes help researchers understand films' physical properties and behaviors and optimize their properties. Several modeling and simulation methods are available for the films, including molecular dynamics simulations, density general function theory, and finite element methods [183–185]. These methods are based on theories and algorithms and apply to different problems and research purposes.

Molecular dynamics (MD) is a computer-simulation technique that can study the structures and behavior of nano-multilayered films. The method is based on Newton's laws of motion and simulates the motion of atoms or molecules in a thin film. Commonly used molecular dynamics software packages include LAMMPS and GROMACS [186–188]. Ding et al. investigated the effects of strain rate and temperature on the mechanical properties of TiN/VN multilayer composites by molecular dynamics, as shown in Fig. 16 (a)–(c) [189]. In Fig. 16 (a), both Young's modulus and inelastic properties show high sensitivity to temperature. In

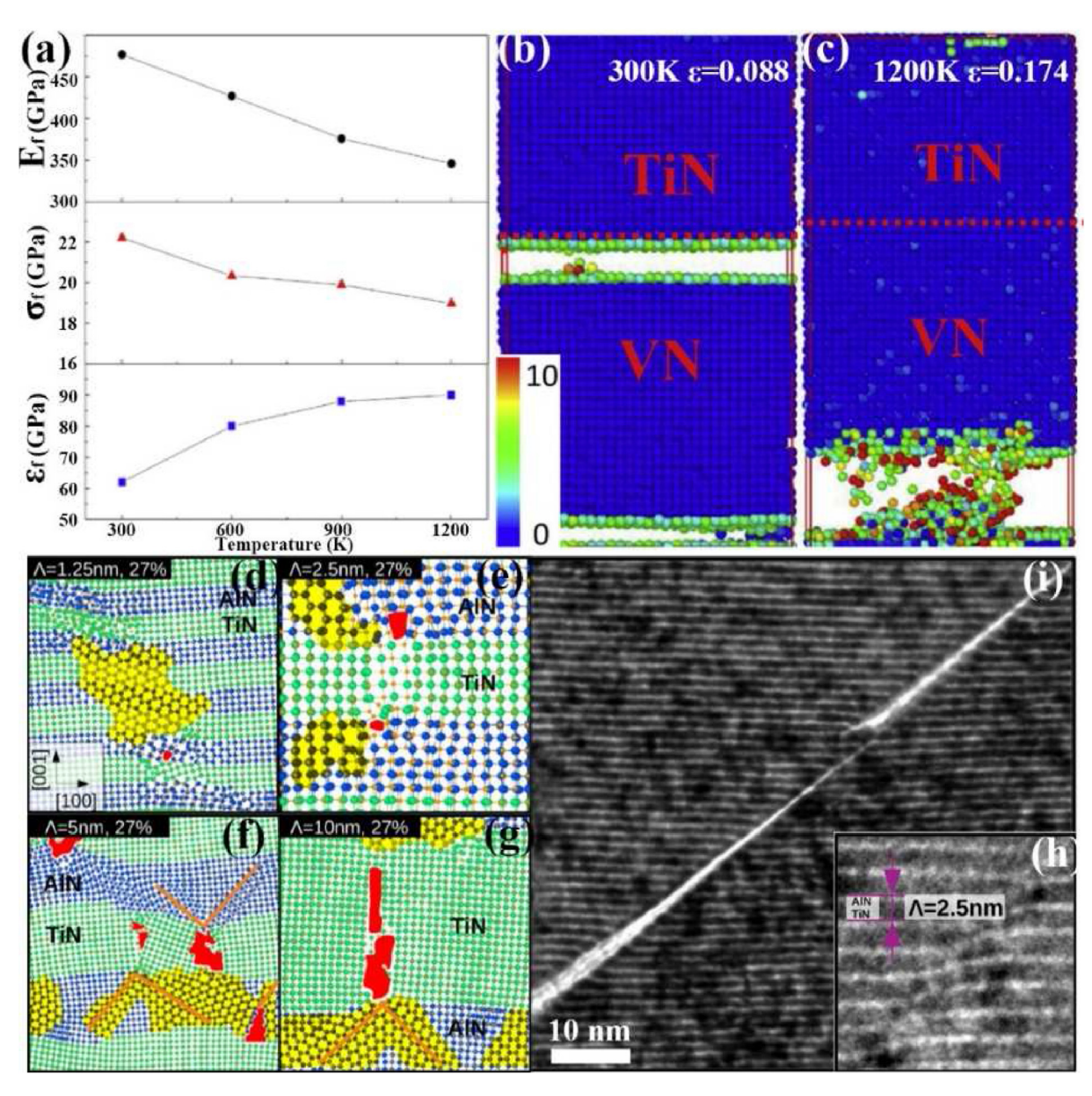


Fig. 16 – (a) Young's modulus (Ef), fracture strength (sf), and fracture strain ( $\epsilon$ f) of TiN/VN composites as a function of temperature, and (b)–(c) its atomic characterization at 300 K ( $\epsilon$  = 0.088) and 1200 K ( $\epsilon$  = 0.174) [189]; (d)–(g) Classical molecular dynamics (CMD) simulations of AlN/TiN SL with various bilayer periods at the interface under strain 27 % (The yellow color highlights structural variations and interfacial discontinuities, the red color labels voids and cracks, while the orange line guides the observation of V-shaped defective pins on the TiN layer); (h)–(i) and its crack extension of TEM images [190].

Fig. 16 (b), the fracture surface exhibits flat and perpendicular to the tensile direction at 300 K, indicating that the damage behavior of TiN/VN composites exhibits typical brittle fracture. In Fig. 16 (c), at 1200 K, the fracture no longer remains flat, indicating that the plasticity of TiN/VN composites increases with increasing temperature, and the fracture behavior gradually changes to ductile fracture. The results show that Young's modulus and fracture strength decrease with increasing temperature while the strain increases. Notably, the fracture behavior occurs only in the VN layer, while the interfacial region and the TiN layer remain stable during uniaxial stretching, indicating that dislocations nucleate only in the soft phase of TiN/VN

composites. The results of molecular dynamics simulations contribute to a better understanding of the hardening mechanism of multilayer coatings. The tensile loading of AlN/TiN SL with a bilayer period  $\Lambda$  varying from 1.25 nm to 10 nm is simulated using classical molecular dynamics as shown in Fig. 16 (d)–(h), aiming to probe the trend of plasticity and fracture resistance with  $\Lambda$  at the atomic level [190]. Compared to  $\Lambda=1.25$  nm in Fig. 16 (d), larger voids at the interface and V-shaped and inclined cracks are observed when  $\Lambda=5$  nm in Fig. 16 (g). At  $\Lambda$  less than 2.5 nm, part of the AlN lattice transition may extend to the TiN layer because the energetic cost of the change in the AlN structure is less than the cost of increasing the interfacial strain,

which helps to dissipate the accumulated stress and improve the toughness. However, when  $\Lambda$  is larger than 5 nm, with the initiation of the partial AlN transition, the Ti-N bonds at the neighboring interfaces undergo localized stretching, which in turn enhances the strain at the AlN/TiN interface, leading to the fracture of the Ti-N bonds and allowing the formation of nano-cracks on the TiN layer. Fig. 16 (i) demonstrates the HRTEM cross-sectional morphology of the nano-indented AlN/TiN SL, where slip/ penetration and diagonal trans-interfacial nano-cracking of the AlN/TiN layer after nanoindentation orthogonal to the interface can be observed. The similarity between simulation predictions and experimental observations is further emphasized. Through electron microscopy studies and molecular dynamics simulations, Zhang et al. explored the multilayer structure mixing behavior of TiN/AlN SL induced by the nanoindentation process [191]. The results show that during nanoindentation loading, the multilayer structure is disrupted and mixed to form a solid solution, reducing the interfacial density and drastically decreasing the dislocation

density. Consequently, the coating properties are degraded. Therefore, the deformation of the multilayer coating during nanoindentation affects its hardness enhancement.

The density general functional theory is a computational method used to calculate nano-multilayered films' electronic structures and properties. The method is based on the concept of the electron-density-distribution function and calculates the electronic structure by solving a system of Kohn-Sham equations [192]. It enables us to understand the phase stability, the formation of defective structures and elastic interfaces, the enhancement of toughness, and the initial stages of oxidation at the atomic scale. It not only provides numerical predictions but also helps reveal physical or chemical origins [193]. Commonly used density available functional theory software packages include VASP [194] and Quantum Espresso [195]. The interfacial interactions of graphene with several orientations of α-alumina have been systematically investigated by first-principles calculations and experiments in Fig. 17 [196]. It is shown that the (0001), (1012), (1011), (1010), and (1102) alumina surfaces do not undergo significant

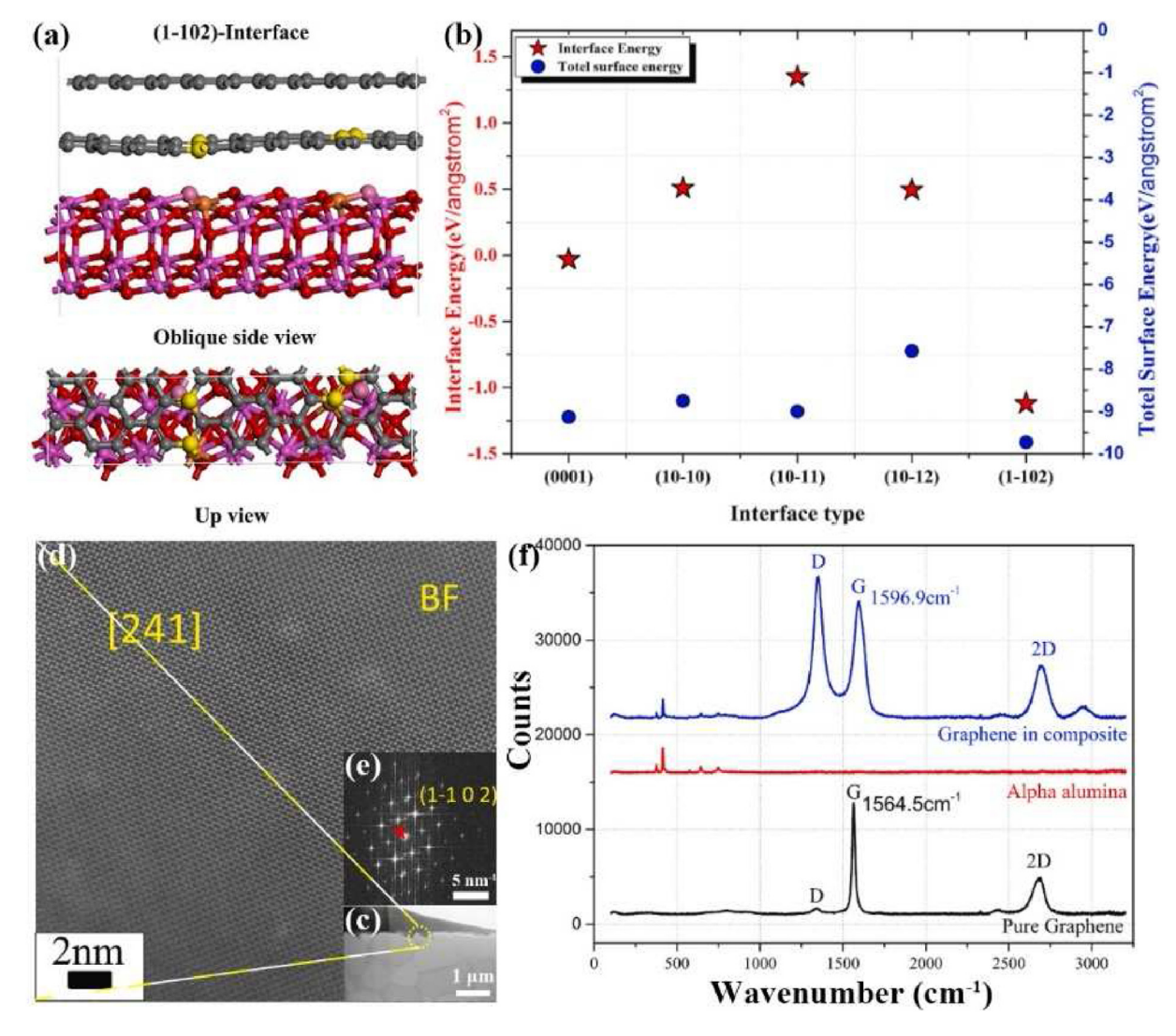


Fig. 17 — (a) schematic of the optimized (1102) interfacial structure (C, Al, and O atoms are represented by yellow, orange, and pink spheres, respectively), (b) interfacial and total surface energies, (c) in-situ FIB sample preparation, (d)—(e) atomic and FFT images of the particles at the interface, (f) Raman spectroscopy analysis results [196].

geometrical reconfiguration with the (0001) graphene surface, whereas the (1011) alumina surface shrinks obviously with the graphene surface. The (1102) alumina surface is the most stable as shown in Fig. 17 (a). The strength of the interfacial electronic interactions is directly related to the stability of the interface through the localized electron density of the states in Fig. 17 (b). In situ high-resolution spherical aberration electron microscopy observation and Raman stress analysis were performed on graphene/alumina interface samples to verify the theoretical calculations in Fig. 17 (c)-(f). It is confirmed that the interface consisting of (1102) surfaces can indeed be stabilized. The finite-element method is a numerical calculation technique used to simulate the mechanical properties of nano-multilayered films. The method divides the film into small cells and solves the mechanical equations in each cell. Popularly used finite-element software packages include ANSYS [197] and COMSOL [198].

In conclusion, modeling and simulations are crucial tools for studying nano-multilayered films. These methods can provide valuable insights into the structures and properties of thin films, which can guide the material design and engineering applications.

#### 6. Conclusion

This paper reviews the basic types, preparation technologies, microstructures, and mechanical properties of nanomultilayered films, which exhibit unique and attractive characteristics. The possible reasons and design criteria for achieving excellent properties are discussed, and proposed research directions for nano-multilayered films are suggested. The main contents of this paper can be summarized as follows:

- (1) Several technologies for the deposition of nanomultilayered films are summarized, including magnetron sputtering, ion plating, chemical-vapor deposition, electrochemical deposition, and other methods. The characteristics of each preparation technique are discussed. Magnetron sputtering has the advantages of broad application, low temperature, and easy manipulation, while arc-ion-plating deposition has the advantages of the high incident particle energy, superior plating density, better strength and durability, and excellent bond strength. Electrodeposition is a versatile technique for preparing nanofilms, in which the electrolyte undergoes a surface reaction during the transport to the substrate.
- (2) The microstructures of nano-multilayered films with phase transformations, interfaces, modulation periods, and ductile metallic phases are discussed. The microstructures of nano-multilayered films affect their material properties. The volume expansion due to the stress-induced transformation of the constituent phases in the modulation layer and the phase transition of the modulation layer by the template effect provide a new way to enhance the mechanical properties of

nano-multilayered films. Coherent interfaces have the same crystal structures and approximate lattice parameters, and dislocations can cross the coherent interfaces. However, small lattice mismatches at the interfaces lead to high coherent stresses, which increase the stiffness of nano-multilayered films. Semicoherent interfaces exhibit high diffusivity and low formation energy and may contain more than one set of interfacial dislocation sites; in turn, dislocations may provide a diffusion pathway to facilitate the diffusion and generation of point defects. "SL films" are formed when the nano-multilayered films obtain the optimum  $\Lambda$ , and two adjacent sublayers grow together at the grain boundaries. Modulated layers with ductility, having a huge slip system, undergo plastic deformation and absorb a large amount of fracture energy during crack extension, which leads to a material with good toughness.

- (3) The mechanical properties of nano-multilayered films, including high hardness and elastic modulus, toughness, temperature and oxidation resistance, and superior wear resistance, are summarized. Multilayers with hard and tough properties represent new high-performance films. Many factors, such as the material composition, *A*, interface structure, residual stress, and dislocation sliding, influence the mechanical behavior of nano-multilayered films. Nano-multilayered films low frictional wear properties provide better application prospects for high-load and long-life friction industries.
- (4) Future work on nano-multilayered films is proposed for the preparation processes, microstructures, models, properties, and applications, which includes the development of new preparation processes, the design of nano-multilayered films with superior hardness and toughness, and the development of modeling and simulations.

# Declaration of competing interest

The authors declare that they have no known competing financial interests or personal relationships that could have appeared to influence the work reported in this paper.

#### Acknowledgments

The authors would like to acknowledge the National Natural Science Foundation of China (Nos. 51971148), the "Dawn" Program of Shanghai Education Commission, China (No. 21SG45), the Shanghai Science and Technology Commission (22010503000) and the Shanghai Engineering Research Center of High-Performance Medical Device Materials (No. 20DZ2 255500). PKL very much appreciates the supports of the U.S. Army Research Office Project (W911NF-13-1-0438 and W911NF-19-2-0049) and the National Science Foundation (DMR-1611180 and 1809640).

#### REFERENCES

- [1] Park HJ, Kim YS, Lee YH, Hong SH, Kim KS, Park YK, et al. Design of nano-scale multilayered nitride hard coatings deposited by arc ion plating process: microstructural and mechanical characterization. J Mater Res Technol 2021;15:572—81. https://doi.org/10.1016/j.jmrt.2021.08.028.
- [2] Li W, Liu P, Liaw PK. Microstructures and properties of highentropy alloy films and coatings: a review. Mater Res Lett 2018;6:199–229. https://doi.org/10.1080/ 21663831.2018.1434248.
- [3] Nasim M, Li YC, Wen M, Wen C. A review of high-strength nanolaminates and evaluation of their properties. J Mater Sci Technol 2020;50:215–44. https://doi.org/10.1016/ j.jmst.2020.03.011.
- [4] Sáenz-Trevizo A, Hodge AM. Nanomaterials by design: a review of nanoscale metallic multilayers. Nanotechnology 2020;31:292002. https://doi.org/10.1088/1361-6528/ab803f.
- [5] Ma ZY, Sun LM, Luo ZB, Lin L, Lei MK. Ultrasonic inverse identification of surface integrity of aviation functional coatings through material-oriented regularization. NDT E Int 2023;133:102733. https://doi.org/10.1016/ j.ndteint.2022.102733.
- [6] Zhang TY, Zhang T, He YT, Wang YC, Bi YP. Corrosion and aging of organic aviation coatings: a review. Chin J Aeronaut 2022;36:1–35. https://doi.org/10.1016/j.cja.2022.12.003.
- [7] Oliveira DR, Granhag L. Ship hull in-water cleaning and its effects on fouling-control coatings. Biofouling 2020;36:332-50. https://doi.org/10.1080/ 08927014.2020.1762079.
- [8] Yin ZZ, Qi WC, Zeng RC, Chen XB, Gu CD, Guan SK, et al. Advances in coatings on biodegradable magnesium alloys. J Magnesium Alloys 2020;8:42-65. https://doi.org/10.1016/ j.jma.2019.09.008.
- [9] Rtimi S, Dionysiou DD, Pillai SC, Kiwi J. Advances in catalytic/photocatalytic bacterial inactivation by nano Ag and Cu coated surfaces and medical devices. Appl Catal B Environ 2019;240:291–318. https://doi.org/10.1016/ j.apcatb.2018.07.025.
- [10] Yao WH, Liang W, Huang GS, Jiang B, Atrens A, Pan FS. Superhydrophobic coatings for corrosion protection of magnesium alloys. J Mater Sci Technol 2020;52:100–18. https://doi.org/10.1016/j.jmst.2020.02.055.
- [11] Mei ZG, Bhattacharya S, Yacout AM. First-principles study of fracture toughness enhancement in transition metal nitrides. Surf Coat Technol 2019;357:903—9. https://doi.org/ 10.1016/j.surfcoat.2018.10.102.
- [12] Kindlund H, Sangiovanni DG, Petrov I, Greene JE, Hultman L. A review of the intrinsic ductility and toughness of hard transition-metal nitride alloy thin films. Thin Solid Films 2019;688:137479. https://doi.org/10.1016/ j.tsf.2019.137479.
- [13] Mbam SO, Nwonu SE, Orelaja OA, Nwigwe US, Gou XF. Thin-film coating; historical evolution, conventional deposition technologies, stress-state micro/nano-level measurement/models and prospects projection: a critical review. Mater Res Express 2019;6:122001.
- [14] Greene JE. Review Article: tracing the recorded history of thin-film sputter deposition: from the 1800s to 2017. J Vac Sci Technol A 2017;35:1–61. https://doi.org/10.1116/ 1.4998940.
- [15] Koehler JS. Attempt to design a strong solid. Phys Rev B 1970;2:547–51. https://doi.org/10.1103/PhysRevB.2.547.
- [16] Yang WMC, Tsakalakos T, Hilliard JE. Enhanced elastic modulus in composition-modulated gold-nickel and copper-palladium foils. J Appl Phys 1977;48:876–9. https:// doi.org/10.1063/1.323749.

- [17] Lehoczky SL. Strength enhancement in thin-layered Al-Cu laminates. J Appl Phys 1978;49:5479–85. https://doi.org/ 10.1063/1.324518.
- [18] Tsakalakos T, Hilliard JE. Elastic modulus in composition-modulated copper-nickel foils. J Appl Phys 1983;54:734–7. https://doi.org/10.1063/1.332083.
- [19] Cammarata RC, Schlesinger TE, Kim C, Qadri SB, Edelstein AS. Nanoindentation study of the mechanical properties of copper-nickel multilayered thin films. Appl Phys Lett 1990;56:1862–4. https://doi.org/10.1063/ 1.103070
- [20] Kowalski W, Paul H, Petrzak P, Maj L, Mania I, Faryna M. Influence of hot pressing on the microstructure of multilayered Ti/Al composites. Arch Metall Mater 2021;66:1149–56. https://doi.org/10.24425/ amm.2021.136435.
- [21] Fu KK, Sheppard L, Chang L, An XH, Yang CH, Ye L. Comparative study on plasticity and fracture behaviour of Ti/Al multilayers. Tribol Int 2018;126:344-51. https:// doi.org/10.1016/j.triboint.2018.05.033.
- [22] Gou XF, Guo ZY, Ma DY, Zhang XM, Li JG, Feng J. Preparation and toughening of a-CuZr/c-ZrN nano-multilayer hard coatings. Appl Surf Sci 2019;483:432–41. https://doi.org/ 10.1016/j.apsusc.2019.03.289.
- [23] Xie WL, Zhao YM, Liao B, Wang S, Zhang S. Comparative tribological behavior of TiN monolayer and Ti/TiN multilayers on AZ31 magnesium alloys. Surf Coat Technol 2022;441:128590. https://doi.org/10.1016/ j.surfcoat.2022.128590.
- [24] Zhou C, Wang JJ, Meng J, Li W, Liu P, Zhang K, et al. Effects of modulation layer thickness on fracture toughness of a TiN/ AlN-Ni multilayer film. Mater Des 2022;222:111097. https:// doi.org/10.1016/j.matdes.2022.111097.
- [25] Wang LP, Qi JL, Cao YQ, Zhang K, Zhang Y, Hao J, et al. Nrich Zr3N4 nanolayers-dependent superhard effect and fracture behavior in TiAlN/Zr<sub>3</sub>N<sub>4</sub> nanomultilayer films. Ceram Int 2020;46:19111–20. https://doi.org/10.1016/j.ceramint.2020.04.246.
- [26] Gao Y, Cai F, Lu X, Xu W, Zhang C, Zhang JZ, et al. Design of cycle structure on microstructure, mechanical properties and tribology behavior of AlCrN/AlCrSiN coatings. Ceram Int 2022;48:12255–70. https://doi.org/10.1016/ j.ceramint.2022.01.087.
- [27] Liu LY, Ma SS, Wu H, Zhu B, Yang HM, Tang JJ, et al. Effect of the annealing process on electrical and optical properties of SnO<sub>2</sub>/Ag/SnO<sub>2</sub> nanometric multilayer film. Mater Lett 2015;149:43–6. https://doi.org/10.1016/j.matlet.2015.02.093.
- [28] Cui WF, Qin GW, Duan JZ, Wang H. A graded nano-TiN coating on biomedical Ti alloy: low friction coefficient, good bonding and biocompatibility. Mater Sci Eng C 2017;71:520–8. https://doi.org/10.1016/j.msec.2016.10.033.
- [29] Liu ZR, Xu YX, Peng B, Wei W, Chen L, Wang QM. Structure and property optimization of Ni-containing AlCrSiN coatings by nano-multilayer construction. J Alloys Compd 2019;808:151630. https://doi.org/10.1016/ j.jallcom.2019.07.342.
- [30] Hasan N, Maity S, Sarkar A, Bhunia CT, Acharjee D, Joseph AM. Simulation and fabrication of SAW-based gas sensor with modified surface state of active layer and electrode orientation for enhanced H<sub>2</sub> gas sensing. J Electron Mater 2016;46:679. https://doi.org/10.1007/s11664-016-5128-7.
- [31] Zhou Q, Ren Y, Du Y, Hua DP, Han WC. Cracking and toughening mechanisms in nanoscale metallic multilayer films: a brief review. Appl Sci 2018;8:1821. https://doi.org/ 10.3390/app8101821.
- [32] Damadam M, Shao S, Ayoub G, Zbib HM. Recent advances in modeling of interfaces and mechanical behavior of

- multilayer metallic/ceramic composites. J Mater Sci 2018;53:5604–17. https://doi.org/10.1007/s10853-017-1704-3.
- [33] Zhang YF, Xue S, Li Q, Li J, Ding J, Niu TJ, et al. Size dependent strengthening in high strength nanotwinned Al/ Ti multilayers. Acta Mater 2019;175:466–76. https://doi.org/ 10.1016/j.actamat.2019.06.028.
- [34] Brandt LR, Salvati E, Wermeille D, Papadaki C, Bourhis E Le, Korsunsky AM. Stress-assisted thermal diffusion barrier breakdown in ion beam deposited Cu/W nano-multilayers on Si substrate observed by in situ GISAXS and transmission EDX. ACS Appl Mater Interfaces 2021;13:6795—804. https://doi.org/10.1021/acsami.0c19173.
- [35] Wang S, Xie MY, Huang HB, Kang M, Liu R, Chen C, et al. Diffusion behavior and bending fracture mechanism of W/ Ti multilayer composites. J Alloys Compd 2021;879:160451. https://doi.org/10.1016/j.jallcom.2021.160451.
- [36] Mishra AK, Gopalan H, Hans M, Kirchlechner C, Schneider JM, Dehm G, et al. Strategies for damage tolerance enhancement in metal/ceramic thin films: lessons learned from Ti/TiN. Acta Mater 2022;228:117777. https://doi.org/10.1016/j.actamat.2022.117777.
- [37] Sen Geng D, Li HQ, Chen ZL, Xu YX, Wang QM. Microstructure, oxidation behavior and tribological properties of AlCrN/Cu coatings deposited by a hybrid PVD technique. J Mater Sci Technol 2022;100:150–60. https:// doi.org/10.1016/j.jmst.2021.06.007.
- [38] Li L, Lu ZX, Pu JX, Hou BR. Investigating the tribological and corrosive properties of MoS2/Zr coatings with the continuous evolution of structure for high-humidity application. Appl Surf Sci 2021;541:148453. https://doi.org/ 10.1016/j.apsusc.2020.148453.
- [39] Ren P, Zhang K, Wen M, Du SX, Chen JH, Zheng WT. The roles of Ag layers in regulating strengthening-toughening behavior and tribochemistry of the Ag/TaC nano-multilayer films. Appl Surf Sci 2018;445:415–23. https://doi.org/ 10.1016/j.apsusc.2018.03.202.
- [40] Kong Y, Tian XB, Gong CZ, Chu PK. Enhancement of toughness and wear resistance by CrN/CrCN multilayered coatings for wood processing. Surf Coat Technol 2018;344:204—13. https://doi.org/10.1016/ j.surfcoat.2018.03.027.
- [41] Ou YX, Ouyang XP, Liao B, Zhang X, Zhang S. Hard yet tough CrN/Si<sub>3</sub>N<sub>4</sub> multilayer coatings deposited by the combined deep oscillation magnetron sputtering and pulsed dc magnetron sputtering. Appl Surf Sci 2020;502:144168. https://doi.org/10.1016/j.apsusc.2019.144168.
- [42] Xiao BJ, Zhang TF, Guo Z, Li Z, Fan B, Chen GX, et al. Mechanical, oxidation, and cutting properties of AlCrN/ AlTiSiN nano-multilayer coatings. Surf Coat Technol 2022;433:128094. https://doi.org/10.1016/ j.surfcoat.2022.128094.
- [43] Zhao CL, Zhu YB, Yuan ZW, Li JL. Structure and tribocorrosion behavior of Ti/TiN multilayer coatings in simulated body fluid by arc ion plating. Surf Coat Technol 2020;403:126399. https://doi.org/10.1016/ j.surfcoat.2020.126399.
- [44] Ma YT, Li L, Qian J, Qu WJ, Luo R, Wu F, et al. Materials and structure engineering by magnetron sputtering for advanced lithium batteries. Energy Storage Mater 2021;39:203–24. https://doi.org/10.1016/j.ensm.2021.04.012.
- [45] Liu M, Yang Y, Mao Q, Wei YQ, Li YJ, Ma NN, et al. Influence of radio frequency magnetron sputtering parameters on the structure and performance of SiC films. Ceram Int 2021;47:24098–105. https://doi.org/10.1016/ j.ceramint.2021.05.120.
- [46] Gudmundsson JT, Brenning N, Lundin D, Helmersson U. High power impulse magnetron sputtering discharge. J Vac

- Sci Technol A 2012;30:030801. https://doi.org/10.1116/1.3691832. -35.
- [47] Betz G, Wien K. Energy and angular distributions of sputtered species. Int J Mass Spectrom Ion Process 1994:140:1–110.
- [48] Tiwari A. Antimicrobial coatings for textiles. Handb. Antimicrob. coatings. Christchurch: Elsevier Inc.; 2017. p. 321–55. https://doi.org/10.1016/B978-0-12-811982-200016-0
- [49] Du HM, Liu P, Li W, Zhang K, Ma FC, Liu XK, et al.  $Al_{80}Cr_{20}N$ -layer thickness-dependent microstructure and mechanical properties of  $Al_{50}Cr_{50}N/Al_{80}Cr_{20}N$  nanomultilayered films. Vacuum 2019;162:1–7. https://doi.org/10.1016/j.vacuum.2019.01.017.
- [50] Cheng WJ, Li W, Wang JJ, Liu P, Ma X, Zhang K, et al. Effects of N<sub>2</sub>/Ar flow ratio on the structures and mechanical behavior of ZrO<sub>x</sub>N<sub>y</sub>/V<sub>2</sub>O<sub>3</sub> nano-multilayered films. Mater Sci Eng, A 2022;849:143419. https://doi.org/10.1016/ j.msea.2022.143419.
- [51] Villamayor A, Pomone T, Perero S, Ferraris M, Barrio VL, G-Berasategui E, et al. Development of photocatalytic nanostructured TiO<sub>2</sub> and NiO/TiO<sub>2</sub> coatings by DC magnetron sputtering for photocatalytic applications. Ceram Int 2023;49:19309. https://doi.org/10.1016/j.ceramint.2023.03.058. -17.
- [52] Beltrami M, Mavrič A, Zilio SD, Fanetti M, Kapun G, Lazzarino M, et al. A comparative study of nanolaminate CrN/Mo<sub>2</sub>N and CrN/W2N as hard and corrosion resistant coatings. Surf Coat Technol 2023:129209. https://doi.org/ 10.1016/j.surfcoat.2022.129209.
- [53] Ku TN, Hsu SY, Lai YT, Chang SY, Tsai SY, Duh JG. Nano-scale mechanical characteristics of epitaxial stabilization ZrTiN/ NbN superlattice coatings. Surf Coat Technol 2023;453:129123. https://doi.org/10.1016/j.surfcoat.2022.129123.
- [54] Gao B, Hu J, Tang S, Xiao XY, Chen HL, Zuo Z, et al. Organicinorganic perovskite films and efficient planar heterojunction solar cells by magnetron sputtering. Adv Sci 2021;8:2102081. https://doi.org/10.1002/advs.202102081.
- [55] Uchida M, Nihira N, Mitsuo A, Toyoda K, Kubota K, Aizawa T. Friction and wear properties of CrAlN and CrVN films deposited by cathodic arc ion plating method. Surf Coat Technol 2004;177:627–30. https://doi.org/10.1016/ S0257-8972(03)00937-X.
- [56] Ikeda T, Satoh H. Phase formation and characterization of hard coatings in the TiAlN system prepared by the cathodic arc ion plating method. Thin Solid Films 1991;195:99–110. https://doi.org/10.1016/0040-6090(91)90262-V.
- [57] Tu R, Yang M, Yuan Y, Min R, Li QZ, Yang MJ, et al. Sandwich structure to enhance the mechanical and electrochemical performance of TaN/(Ta/Ti)/TiN multilayer films prepared by multi-arc ion plating. Coatings 2022;12:694. https://doi.org/10.3390/coatings12050694.
- [58] Xian LJ, Zhao HB, Xian G, Fan HY, Xiong J. Oxidation resistance and thermal insulation performance of thin nano-multilayered (Al,Cr)<sub>2</sub>O<sub>3</sub>/ZrO<sub>2</sub> coating prepared by arc ion plating technique. Mater Lett 2020;281:128649. https:// doi.org/10.1016/j.matlet.2020.128649.
- [59] Hu XG, Qiu LS, Pan XL, Zhang JC, Li XN, Zhang S, et al. Nitrogen diffusion mechanism, microstructure and mechanical properties of thick Cr/CrN multilayer prepared by arc deposition system. Vacuum 2022;199:110902. https:// doi.org/10.1016/j.vacuum.2022.110902.
- [60] Ma HR, Miao Q, Zhang GH, Liang WP, Wang Y, Sun ZW, et al. The influence of multilayer structure on mechanical behavior of TiN/TiAlSiN multilayer coating. Ceram Int 2021;47:12583–91. https://doi.org/10.1016/j.ceramint .2021.01.117.

- [61] zhao Sun L, Yuan GW, Gao LB, Yang JU, Chhowalla M, Gharahcheshmeh MH, et al. Chemical vapour deposition. Nat Rev Methods Prim 2021;1:5. https://doi.org/10.1038/ s43586-020-00005-y.
- [62] Kim HM, Choi SC, Kim Y, Lee HI, Choi K. Thermal shock resistance of TaC/SiC coatings on carbon/carbon composites by the CVD process. J Ceram Process Res 2020;21:92–8. https://doi.org/10.36410/jcpr.2020.21.1.92.
- [63] Shan JJ, Li JH, Chu XY, Xu MZ, Jin FJ, Fang X, et al. Enhanced photoresponse characteristics of transistors using CVDgrown MoS<sub>2</sub>/WS<sub>2</sub> heterostructures. Appl Surf Sci 2018;443:31–8. https://doi.org/10.1016/j.apsusc.2018.02.244.
- [64] Kainz C, Schalk N, Tkadletz M, Mitterer C, Czettl C. Microstructure and mechanical properties of CVD TiN/TiBN multilayer coatings. Surf Coat Technol 2019;370:311–9. https://doi.org/10.1016/j.surfcoat.2019.04.086.
- [65] Shen TW, Zhu LH, Liu ZY. Effect of micro-blasting on the tribological properties of TiN/MT-TiCN/Al<sub>2</sub>O<sub>3</sub>/TiCNO coatings deposited by CVD. Int J Refract Met Hard Mater 2020;88:105205. https://doi.org/10.1016/ j.ijrmhm.2020.105205.
- [66] Tsavdaris N, Harza D, Coindeau S, Renou G, Robaut F, Jacquemin M, et al. A chemical vapor deposition route to epitaxial superconducting NbTiN thin films. Chem Mater 2017;29:5824–30. https://doi.org/10.1021/ acs.chemmater.7b00490.
- [67] Shi Y, Huang WM, Li J, Zhou Y, Li ZQ, Yin YC, et al. Site-specific electrodeposition enables self-terminating growth of atomically dispersed metal catalysts. Nat Commun 2020;11:4558. https://doi.org/10.1038/s41467-020-18430-8.
- [68] Saidin NU, Ying KK, Khuan NI. Electrodeposition: principles, applications and methods, vols. 1–5; 2011.
- [69] Jayakrishnan DS. Electrodeposition: the versatile technique for nanomaterials. Corros. Prot. Control Using Nanomater. Woodhead Publishing Limited; 2012. p. 86–125. https:// doi.org/10.1533/9780857095800.1.86.
- [70] Karimzadeh A, Rouhaghdam AS, Aliofkhazraei M, Miresmaeili R. Sliding wear behavior of Ni-Co-P multilayer coatings electrodeposited by pulse reverse method. Tribiology Int 2020;141:105914. https://doi.org/10.1016/ j.triboint.2019.105914.
- [71] Chen YS, Lin CC, Chin TS, Chang JY, Sung CK. Residual stress analysis of electrodeposited thick CoMnP monolayers and CoMnP/Cu multilayers. Surf Coat Technol 2022;434:128169. https://doi.org/10.1016/ j.surfcoat.2022.128169.
- [72] Fu ZR, Zhang Z, Meng LF, Shu BP, Zhu YT, Zhu XK. Effect of strain rate on mechanical properties of Cu/Ni multilayered composites processed by electrodeposition. Mater Sci Eng, A 2018;726:154–9. https://doi.org/10.1016/j.msea.2018.04.076.
- [73] Guo HX, Sun QS, Zhou DP, Yu M, Wang YX, Wang Q, et al. Erosion behavior of CrN, CrAlN and CrAlN/CrN multilayer coatings deposited on Ti6Al4V. Surf Coat Technol 2022;437:128284. https://doi.org/10.1016/ j.surfcoat.2022.128284.
- [74] Shuai JT, Zuo X, Wang ZY, Sun LL, Chen R De, Wang L, et al. Erosion behavior and failure mechanism of Ti/TiAlN multilayer coatings eroded by silica sand and glass beads. J Mater Sci Technol 2021;80:179–90. https://doi.org/10.1016/ j.jmst.2021.01.001.
- [75] Wan Q, Yang B, Liu HD, Chen J, Zhang J. Microstructure and adhesion of MeN/TiSiN (Me = Ti, Cr, Zr, Mo, Nb<sub>x</sub>Al<sub>1-x</sub>) multilayered coatings deposited by cathodic arc ion plating. Appl Surf Sci 2019;497:143602. https://doi.org/10.1016/ j.apsusc.2019.143602.
- [76] Liu DG, Ruan CF, Zhang P, Ma HR, Liang Y, Tu JP. Structural, interface texture and toughness of TiAlN/ $CN_x$  multilayer

- films. Mater Char 2021;178:111301. https://doi.org/10.1016/j.matchar.2021.111301.
- [77] Yan HJ, Tian QY, Gao DW, Yang FF. Microstructure and properties of TiAlN/AlN multilayers with different modulation periods. Surf Coat Technol 2019;363:61–5. https://doi.org/10.1016/j.surfcoat.2019.01.064.
- [78] Wang T, Zhang GJ, Jiang BL. Microstructure, mechanical and tribological properties of TiMoN/Si3N4 nano-multilayer films deposited by magnetron sputtering. Appl Surf Sci 2015;326:162-7. https://doi.org/10.1016/ j.apsusc.2014.11.125.
- [79] Kim DJ, Truong QT, Kim JI, Suh YJ, Moon JH, Lee SE, et al. Ultrahigh-strength multi-layer graphene-coated Ni film with interface-induced hardening. Carbon 2021;178:497–505. https://doi.org/10.1016/ j.carbon.2021.03.021.
- [80] Ashkinazi EE, Ryzhkov SG, Martyanov AK, Bolshakov AP, Sergeichev KF, Shevchenko MY, et al. Temperature stabilization of WC-Co cutting inserts with feedback to IR pyrometer upon growth of multilayer diamond coatings by microwave plasma chemical vapor deposition. Mater Today Proc 2021;38:1495–501. https://doi.org/10.1016/ j.matpr.2020.08.136.
- [81] Liu B, Tang B, Lv FJ, Zeng Y, Liao JH, Wang S, et al. Photodetector based on heterostructure of two-dimensional WSe<sub>2</sub>/In<sub>2</sub>Se<sub>3</sub>. Nanotechnology 2020;31:065203. https:// doi.org/10.1088/1361-6528/ab519b.
- [82] Grützmacher PG, Suarez S, Tolosa A, Gachot C, Song GC, Wang B, et al. Superior wear-resistance of Ti<sub>3</sub>C<sub>2</sub>T<sub>x</sub> multilayer coatings. ACS Nano 2021;15:8216–24. https://doi.org/10.1021/acsnano.1c01555.
- [83] Stambolova I, Dimitrov O, Vassilev S, Yordanov S, Blaskov V, Boshkov N, et al. Preparation of newly developed CeO<sub>2</sub>/ZrO<sub>2</sub> multilayers: effect of the treatment temperature on the structure and corrosion performance of stainless steel. J Alloys Compd 2019;806:1357–67. https://doi.org/ 10.1016/j.jallcom.2019.07.308.
- [84] Felizco J, Uenuma M, Juntunen T, Etula J, Tossi C, Ishikawa Y, et al. Enhanced thermoelectric transport and stability in atomic layer deposited-HfO<sub>2</sub>/ZnO and TiO<sub>2</sub>/ZnOsandwiched multilayer thin films. ACS Appl Mater Interfaces 2020;12:49210-8. https://doi.org/10.1021/ acsami.0c11439.
- [85] Sproul WD. New routes in the preparation of mechanically hard films. Science 1996;273:889–92.
- [86] Chen YM, Guo T, Wang JW, Pang XL, Qiao LJ. Effects of orientation on microstructure and mechanical properties of TiN/AlN superlattice films. Scripta Mater 2021;201:113951. https://doi.org/10.1016/j.scriptamat.2021.113951.
- [87] Liu Y, Liu HD, Pelenovich V, Wan Q, Guo JL, Chen YM, et al. Influences of modulation period on structure and properties of AlTiSiN/AlCrSiN nanocomposite multilayer coatings. Vacuum 2021;193:110516. https://doi.org/10.1016/ j.vacuum.2021.110516.
- [88] Kravchenko YO, Coy E, Peplińska B, Iatsunskyi I, Załęski K, Kempiński M, et al. Micro-mechanical investigation of (Al<sub>50</sub>Ti<sub>50</sub>)N coatings enhanced by ZrN layers in the nanolaminate architecture. Appl Surf Sci 2020;534:147573. https://doi.org/10.1016/j.apsusc.2020.147573.
- [89] Zuo B, Xu JH, Lu GY, Ju HB, Yu LH. Microstructures, mechanical properties and corrosion resistance of TiN/AlN multilayer films. Ceram Int 2022;48:11629–35. https:// doi.org/10.1016/j.ceramint.2022.01.020.
- [90] Yalamanchili K, Schramm IC, Pique EJ, Rogström L, Mücklich F, Oden M, et al. Tuning hardness and fracture resistance of ZrN/Zr<sub>0.63</sub>Al<sub>0.37</sub>N nanoscale multilayers by stress-induced transformation toughening. Acta Mater

- 2015;89:22-31. https://doi.org/10.1016/j.actamat.2015.01.066.
- [91] Wang C, Han J, Pureza JM, Chung YW. Structure and mechanical properties of  $Fe_{1-x}Mnx/TiB_2$  multilayer coatings: possible role of transformation toughening. Surf Coat Technol 2013;237:158–63. https://doi.org/10.1016/j.surfcoat.2013.08.014.
- [92] Zhang YF, Li Q, Gong M, Xue S, Ding J, Li J, et al. Deformation behavior and phase transformation of nanotwinned Al/Ti multilayers. Appl Surf Sci 2020;527:146776. https://doi.org/ 10.1016/j.apsusc.2020.146776.
- [93] Pan YP, Dong L, Liu N, Yu JG, Li C, Li DJ. Investigating the influence of epitaxial modulation on the evolution of superhardness of the VN/TiB<sub>2</sub> multilayers. Appl Surf Sci 2016;390:406–11. https://doi.org/10.1016/ j.apsusc.2016.08.133.
- [94] Du JW, Chen L, Chen J, Du Y. Mechanical properties, thermal stability and oxidation resistance of TiN/CrN multilayer coatings. Vacuum 2020;179:109468. https:// doi.org/10.1016/j.vacuum.2020.109468.
- [95] Ma YH, Wang ZG, Ouyang JH, Dillon SJ, Henniche A, Wang YH, et al. Microstructural toughening mechanisms in nanostructured Al<sub>2</sub>O<sub>3</sub>/GdAlO<sub>3</sub> eutectic composite studied using in situ microscale fracture experiments. J Eur Ceram Soc 2020;40:3148–57. https://doi.org/10.1016/ j.jeurceramsoc.2020.02.042.
- [96] Shi JM, Hashimoto N, Isobe S. Cohesion properties of incoherent Fe/W interfaces: a DFT study. J Nucl Mater 2021;549:152858. https://doi.org/10.1016/ j.jnucmat.2021.152858.
- [97] Ren QQ, Fan JL, Gong HR. Work function and cohesion properties of W-Fe interfaces. Mater Lett 2015;145:205–8. https://doi.org/10.1016/j.matlet.2015.01.082.
- [98] Chen Z, Shao QQ, Bartosik M, Mayrhofer PH, Chen H, Zhang ZL. Growth-twins in CrN/AlN multilayers induced by hetero-phase interfaces. Acta Mater 2020;185:157–70. https://doi.org/10.1016/j.actamat.2019.11.063.
- [99] Yang W, Ayoub G, Salehinia I, Mansoor B, Zbib H. Multiaxial tension/compression asymmetry of Ti/TiN nano laminates: MD investigation. Acta Mater 2017;135:348–60. https://doi.org/10.1016/j.actamat.2017.06.034.
- [100] Kim Jae-Il, Kim Jongkuk, Kim Do Hyun, Young-Jun Jang NU. Improved wear imbalance with multilayered nanocomposite nanocrystalline Cu and tetrahedral amorphous carbon coating. Ceram Int 2021;47:25664-73. https://doi.org/10.1016/j.ceramint.2021.05.292.
- [101] Levitas VI. Phase transformations, fracture, and other structural changes in inelastic materials. Int J Plast 2021;140:102914. https://doi.org/10.1016/ j.ijplas.2020.102914.
- [102] Sangiovanni DG. Inherent toughness and fracture mechanisms of refractory transition-metal nitrides via density-functional molecular dynamics. Acta Mater 2018;151:11–20. https://doi.org/10.1016/ j.actamat.2018.03.038.
- [103] Maksakova OV, Webster RF, Tilley RD, Ivashchenko VI, Postolnyi BO, Bondar OV, et al. Nanoscale architecture of (CrN/ZrN)/(Cr/Zr) nanocomposite coatings: microstructure, composition, mechanical properties and first-principles calculations. J Alloys Compd 2020;831:154808. https:// doi.org/10.1016/j.jallcom.2020.154808.
- [104] Guo SK, Sun H. Superhardness induced by grain boundary vertical sliding in (001)-textured ZrB<sub>2</sub> and TiB<sub>2</sub> nano films. Acta Mater 2021;218:117212. https://doi.org/10.1016/ j.actamat.2021.117212.
- [105] Wang T, Jin YL, Bai LJ, Zhang GJ. Structure and properties of NbN/Mon nano-multilayer coatings deposited by

- magnetron sputtering. J Alloys Compd 2017;729:942–8. https://doi.org/10.1016/j.jallcom.2017.09.218.
- [106] Buchinger JL, Koutná N, Chen Z, Zhang ZL, Mayrhofer PH, Holec D, et al. Toughness enhancement in TiN/WN superlattice thin films. Acta Mater 2019;172:18–29. https:// doi.org/10.1016/j.actamat.2019.04.028.
- [107] Chen Z, Zheng Y, Huang Y, Gao Z, Sheng H, Bartosik M, et al. Atomic-scale understanding of the structural evolution in TiN/AlN superlattice during nanoindentation—Part 2: strengthening. Acta Mater 2022;234:118009. https://doi.org/ 10.1016/j.actamat.2022.118009.
- [108] Helmersson U, Todorova S, Barnett SA, Sundgren JE, Markert LC, Greene JE. Growth of single-crystal TiN/VN strained-layer superlattices with extremely high mechanical hardness. J Appl Phys 1987;62:481–4. https:// doi.org/10.1063/1.339770.
- [109] Ljungcrantz H, Engström C, Hultman L, Olsson M, Chu X, Wong MS, et al. Nanoindentation hardness, abrasive wear, and microstructure of TiN/NbN polycrystalline nanostructured multilayer films grown by reactive magnetron sputtering. J Vac Sci Technol A 1998;16:3104–13. https://doi.org/10.1116/1.581466.
- [110] Li GY, Li GQ, Li YG. Crystallization of amorphous AlN and superhardness effect in VC/AlN nanomultilayers. Thin Solid Films 2012;520:2032–5. https://doi.org/10.1016/ j.tsf.2011.09.079.
- [111] Pogrebnjak AD, Beresnev VM, Bondar OV, Postolnyi BO, Zaleski K, Coy E, et al. Superhard CrN/Mon coatings with multilayer architecture. Mater Des 2018;153:47–59. https:// doi.org/10.1016/j.matdes.2018.05.001.
- [112] Avila PRT, Silva EPD, Rodrigues AM, Aristizabal K, Pineda F, Coelho RS, et al. On manufacturing multilayer-like nanostructures using misorientation gradients in PVD films. Sci Rep 2019;9:15898. https://doi.org/10.1038/s41598-019-52226-1.
- [113] Veprek S, Veprek-Heijman MGJ, Karvankova P, Prochazka J. Different approaches to superhard coatings and nanocomposites. Thin Solid Films 2005;476:1–29. https:// doi.org/10.1016/j.tsf.2004.10.053.
- [114] Musil J. Hard and superhard nanocomposite coatings. Surf Coat Technol 2000;125:322—30. https://doi.org/10.1016/ S0257-8972(99)00586-1.
- [115] Oliver WC, Pharr GM. An improved technique for determining hardness and elastic modulus using load and displacement sensing indentation experiments. J Mater Res 1992;7:1564–83. https://doi.org/10.1557/JMR.1992.1564.
- [116] Postolnyi BO, Beresnev VM, Abadias G, Bondar OV, Rebouta L, Araujo JP, et al. Multilayer design of CrN/Mon protective coatings for enhanced hardness and toughness. J Alloys Compd 2017;725:1188–98. https://doi.org/10.1016/ j.jallcom.2017.07.010.
- [117] Du SX, Zhang K, Wen M, Ren P, Meng QN, Zhang YD, et al. Crystallization of SiC and its effects on microstructure, hardness and toughness in TaC/SiC multilayer films. Ceram Int 2018;44:613–21. https://doi.org/10.1016/ j.ceramint.2017.09.220.
- [118] Bai XB, Li JL, Zhu LH. Structure and properties of TiSiN/Cu multilayer coatings deposited on Ti6Al4V prepared by arc ion plating. Surf Coat Technol 2019;372:16–25. https:// doi.org/10.1016/j.surfcoat.2019.05.013.
- [119] Kong M, Wu XY, Huang BL, Li GY. Epitaxial growth and superhardness effect of TiN/AlON nanomultilayers synthesized by reactive magnetron sputtering technology. J Alloys Compd 2009;485:435–8. https://doi.org/10.1016/ j.jallcom.2009.05.133.
- [120] Li YG, Li GQ, Yang D, Li GY. Microstructure evolution and mechanical properties in VC/SiC nanomultilayers. Appl

- Surf Sci 2012;258:9856-8. https://doi.org/10.1016/j.apsusc.2012.06.042.
- [121] Chen WL, Yan A, Wang CY, Deng Y, Chen DC, Xiao H, et al. Microstructures and mechanical properties of AlCrN/TiSiN nanomultilayer coatings consisting of fcc single-phase solid solution. Appl Surf Sci 2020;509:145303. https://doi.org/ 10.1016/j.apsusc.2020.145303.
- [122] Chen XJ, Du Y, Chung YW. Commentary on using H/E and H<sup>3</sup>/E<sup>2</sup> as proxies for fracture toughness of hard coatings. Thin Solid Films 2019;688:137265. https://doi.org/10.1016/j.tsf.2019.04.040.
- [123] Greenwood JA, Williamson JP. Contact of nominally flat surfaces, vol. 295. Series A. Proceedings of the royal society of London; 1964.
- [124] Johnson KL. Contact mechanics. London, UK: Cambridge university press; 1987.
- [125] Lawn BR, Evans AG, Marshall DB. Elastic/plastic indentation damage in ceramics: the median/radial crack system. J Am Ceram Soc 1980;63:574–81. https://doi.org/10.1111/j.1151-2916.1980.tb10768.x.
- [126] Zhu XK, Joyce JA. Review of fracture toughness (G, K, J, CTOD, CTOA) testing and standardization. Eng Fract Mech 2012;85:1–46. https://doi.org/10.1016/ j.engfracmech.2012.02.001.
- [127] Li XD, Diao DF, Bhushan B. Fracture mechanisms of thin amorphous carbon films in nanoindentation. Acta Mater 1997;45:4453–61. https://doi.org/10.1016/S1359-6454(97) 00143-2.
- [128] Kabir MS, Zhou ZF, Xie ZH, Munroe P. Designing multilayer diamond like carbon coatings for improved mechanical properties. J Mater Sci Technol 2021;65:108–17. https:// doi.org/10.1016/j.jmst.2020.04.077.
- [129] Zeng C, Pu J Bin, Wang HX, Zheng SJ, Chen R. Influence of microstructure on tribological properties and corrosion resistance of MoS<sub>2</sub>/WS<sub>2</sub> films. Ceram Int 2020;46:13774–83. https://doi.org/10.1016/j.ceramint.2020.02.167.
- [130] Zhang Q, Xu YX, Zhang TF, Wu ZT, Wang QM. Tribological properties, oxidation resistance and turning performance of AlTiN/AlCrSiN multilayer coatings by arc ion plating. Surf Coat Technol 2018;356:1–10. https://doi.org/10.1016/ j.surfcoat.2018.09.027.
- [131] Miletić A, Panjan P, Čekada M, Kovačević L, Terek P, Kovač J, et al. Nanolayer CrAlN/TiSiN coating designed for tribological applications. Ceram Int 2021;47:2022–33. https://doi.org/10.1016/j.ceramint.2020.09.034.
- [132] Wu ZT, Ye RL, Bakhit B, Petrov I, Hultman L, Greczynski G. Improving oxidation and wear resistance of TiB<sub>2</sub> films by nano-multilayering with Cr. Surf Coat Technol 2022;436:128337. https://doi.org/10.1016/ j.surfcoat.2022.128337.
- [133] Zhang GJ, Fan TX, Wang T, Chen HL. Microstructure, mechanical and tribological behavior of MoN<sub>x</sub>/SiN<sub>x</sub> multilayer coatings prepared by magnetron sputtering. Appl Surf Sci 2013;274:231–6. https://doi.org/10.1016/ j.apsusc.2013.03.021.
- [134] Jasempoor F, Elmkhah H, Imantalab O, Fattah-alhosseini A. Improving the mechanical, tribological, and electrochemical behavior of AISI 304 stainless steel by applying CrN single layer and Cr/CrN multilayer coatings. Wear 2022;504(505):204425. https://doi.org/10.1016/ j.wear.2022.204425.
- [135] Zhao GL, Wang JH, Deng YY, Yan TT, Liang WF, Li T, et al. The study of the tribological properties of TiB<sub>2</sub>/Cr multilayered coatings over a wide temperature range. J Mater Res Technol 2022;16:290–301. https://doi.org/10.1016/ j.jmrt.2021.11.158.
- [136] Tian CX, Han B, Zou CW, Xie X, Li SQ, Liang F, et al. Synthesis of monolayer  $MoN_{\rm x}$  and nanomultilayer CrN/

- Mo<sub>2</sub>N coatings using arc ion plating. Surf Coat Technol 2019;370:125–9. https://doi.org/10.1016/j.surfcoat.2019.03.014.
- [137] Elias L, Bhat KU, Hegde AC. Development of nanolaminated multilayer Ni-P alloy coatings for better corrosion protection. RSC Adv 2016;6:34005—13. https://doi.org/ 10.1039/c6ra01547f.
- [138] Rahsepar M, Bahrololoom ME. Corrosion study of Ni/Zn compositionally modulated multilayer coatings using electrochemical impedance spectroscopy. Corrosion Sci 2009;51:2537–43. https://doi.org/10.1016/ j.corsci.2009.06.030.
- [139] Cai F, Zhou Q, Chen JK, Zhang SH. Effect of inserting the Zr layers on the tribo-corrosion behavior of Zr/ZrN multilayer coatings on titanium alloys. Corrosion Sci 2023;213:111002. https://doi.org/10.1016/j.corsci.2023.111002.
- [140] Mani SP, Agilan P, Kalaiarasan M, Ravichandran K, Rajendran N, Meng Y. Effect of multilayer CrN/CrAlN coating on the corrosion and contact resistance behavior of 316L SS bipolar plate for high temperature proton exchange membrane fuel cell. J Mater Sci Technol 2022;97:134—46. https://doi.org/10.1016/j.jmst.2021.04.043.
- [141] Wang R, Li HQ, Li RS, Mei HJ, Zou CW, Zhang TF, et al. Thermostability, oxidation, and high-temperature tribological properties of nano-multilayered AlCrSiN/VN coatings. Ceram Int 2022;48:11915–23. https://doi.org/ 10.1016/j.ceramint.2022.01.041.
- [142] Mao YR, Chen YM, Zhang Q, Wang RP, Shen X. Improvement of thermal stability and phase change behavior of  $Ge_2Sb_2Te_5$  thin films by Calcium doping. J Non-Cryst Solids 2020;549:120338–44. https://doi.org/10.1016/j.jnoncrysol.2020.120338.
- [143] Zhang K, Lei SY, Yang RX, Zhang YC, Chen SH, Zhang XH, et al. Formation and oxidation behavior of SiO<sub>2</sub>/NbSi<sub>2</sub> multilayer coating fabricated by one-step method. Surf Coat Technol 2023;452:129117. https://doi.org/10.1016/ j.surfcoat.2022.129117.
- [144] Li H, Ma DY, Wang HB, Yun D, Hao Z, Deng JK, et al. Microstructure and oxidation behavior of CrCN/TiSiCN nano-multilayer coatings on Zircaloy in high-temperature steam. Corrosion Sci 2023;211:110883. https://doi.org/ 10.1016/j.corsci.2022.110883.
- [145] Ju H, Xu L, Luan J, Geng Y, Xu J, Yu L, et al. Enhancement on the hardness and oxidation resistance property of TiN/Ag composite films for high temperature applications by addition of Si. Vacuum 2023;209:111752. https://doi.org/ 10.1016/j.vacuum.2022.111752.
- [146] Liu JK, Hao Z, Cui ZX, Ma DY, Lu JQ, Cui YG, et al. Investigation of the oxidation mechanisms of superlattice Cr-CrN/TiSiN-Cr multilayer coatings on Zircaloy substrates under high-temperature steam atmospheres. Corrosion Sci 2021;192:109782. https://doi.org/10.1016/ j.corsci.2021.109782.
- [147] Tytko D, Choi PP, Raabe D. Oxidation behavior of ALN/CRN multilayered hard coatings. Nano Converg 2017;4:1–5. https://doi.org/10.1186/s40580-017-0109-y.
- [148] Monclús MA, Callisti M, Polcar T, Yang LW, Llorca J, Molina-Aldareguía JM. Selective oxidation-induced strengthening of Zr/Nb nanoscale multilayers. Acta Mater 2017;122:1–10. https://doi.org/10.1016/j.actamat.2016.09.021.
- [149] Moszner F, Cancellieri C, Chiodi M, Yoon S, Ariosa D, Janczak-Rusch J, et al. Thermal stability of Cu/W nanomultilayers. Acta Mater 2016;107:345-53. https://doi.org/ 10.1016/j.actamat.2016.02.003.
- [150] He YX, Wang XB, Guo T, Gao KW, Pang XL. Effect of interface on oxidation behavior and tribological properties of CrAlN/SiNx multilayer films. Ceram Int 2022;49:1369–80. https://doi.org/10.1016/j.ceramint.2022.09.118.

- [151] Zhang C, Feng K, Li ZG, Lu FG, Huang J, Wu YX, et al. Enhancement of high-temperature strength of Ni-based films by addition of nano-multilayers and incorporation of W. Acta Mater 2017;133:55-67. https://doi.org/10.1016/ j.actamat.2017.05.037.
- [152] Holger Schwarz TU, Rösch Niels, Lindner Thomas, Lampke Thomas, Fabian Ganss OH. CoCrFeNi high-entropy alloy thin films synthesised by magnetron sputter deposition from spark plasma sintered targets. Coatings 2021;11. https://doi.org/10.3390/coatings11040468.
- [153] Cui PP, Li W, Liu P, Wang JJ, Ma X, Zhang K, et al. The influence of WS<sub>2</sub> layer thickness on microstructures and mechanical behavior of high-entropy (AlCrTiZrNb)N/WS<sub>2</sub> nanomultilayered films. Surf Coat Technol 2022;433:128091. https://doi.org/10.1016/j.surfcoat.2022.128091.
- [154] Zhai Q, Li W, Liu P, Cheng W, Zhang K, Ma F, et al. Mechanical behavior and thermal stability of (AlCrTiZrMo) N/ZrO<sub>2</sub> nano-multilayered high-entropy alloy film prepared by magnetron sputtering. Crystals 2022;12:232. https:// doi.org/10.3390/cryst12020232.
- [155] Cui PP, Li W, Liu P, Zhang K, Ma FC, Chen XH, et al. Effects of nitrogen content on microstructures and mechanical properties of (AlCrTiZrHf)N high-entropy alloy nitride films. J Alloys Compd 2020;834:155063. https://doi.org/10.1016/ j.jallcom.2020.155063.
- [156] Lin SS, Zhou KS, Dai MJ, Hu F, Shi Q, Hou HJ, et al. Effects of surface roughness of substrate on properties of Ti/TiN/Zr/ZrN multilayer coatings. Trans Nonferrous Met Soc China 2015;25:451–6. https://doi.org/10.1016/S1003-6326(15)63623-8.
- [157] Cao HS, Ye X, Li H, Qi FQ, Wang Q, Ouyang XP, et al. Microstructure, mechanical and tribological properties of multilayer Ti-DLC thick films on Al alloys by filtered cathodic vacuum arc technology. Mater Des 2021;198:109320. https://doi.org/10.1016/ j.matdes.2020.109320.
- [158] Dang CQ, Yao YR, Olugbade T, Li JL, Wang LP. Effect of multi-interfacial structure on fracture resistance of composite TiSiN/Ag/TiSiN multilayer coating. Thin Solid Films 2018;653:107–12. https://doi.org/10.1016/ i.tsf.2018.03.029.
- [159] Yuan ZY, Guo YN, Li CH, Liu LS, Yang B, Song HZ, et al. New multilayered diamond/β-SiC composite architectures for high-performance hard coating. Mater Des 2020;186:108207. https://doi.org/10.1016/j.matdes.2019.108207.
- [160] Penkov OV, Khadem M, Kim DE. Hard, flexible, and transparent nanolayered SiN<sub>x</sub>/BN periodical coatings. ACS Appl Mater Interfaces 2019;11:9685–90. https://doi.org/ 10.1021/acsami.8b22091.
- [161] Anderson PM, Li C. Hall-Petch realstions for multilayered materials. Nanostruct Mater 1995;5:349–62. https://doi.org/ 10.1016/0965-9773(95)00250-I.
- [162] Li GY, Han ZH, Tian JW, Xu JH, Gu MY. Alternating stress field and superhardness effect in TiN/NbN superlattice films. J Vac Sci Technol A 2002;20:674—7. https://doi.org/ 10.1116/1.1460887.
- [163] Pacheco ES, Mura T. Interaction between a screw dislocation and a bimetallic interface. J Mech Phys Solid 1969;17:163-70. https://doi.org/10.1016/0022-5096(69)90030-1.
- [164] Chu X, Barnett SA. Model of superlattice yield stress and hardness enhancements. J Appl Phys 1995;77:4403–11. https://doi.org/10.1063/1.359467.
- [165] Kato M, Mori T, Schwartz LH. Hardening by spinodal modulated structure. Acta Metall 1980;28:285–90. https:// doi.org/10.1016/0001-6160(80)90163-7.
- [166] Shinn M, Barnett SA. Effect of superlattice layer elastic moduli on hardness. Appl Phys Lett 1994;64:61–3. https:// doi.org/10.1063/1.110922.

- [167] Hall EO. The deformation and ageing of mild steel: II Characteristics of the Lüders deformation. Proc Phys Soc 1951;64:742. https://doi.org/10.1088/0370-1301/64/9/302. Bristol, England: IOP Publishing Ltd.
- [168] Ryou H, Drazin JW, Wahl KJ, Qadri SB, Gorzkowski EP, Feigelson BN, et al. Below the Hall-Petch limit in nanocrystalline ceramics. ACS Nano 2018;12:3083–94. https://doi.org/10.1021/acsnano.7b07380.
- [169] Lu C, Meng F, Liu H, Lei X, Yang J, Huang J, et al. Influence of interfacial configuration on superhardness effect in TiN (111)/NbN (111) nano-multilayer film: a first-principles calculation. Mater Today Commun 2020;24:1—11. https:// doi.org/10.1016/j.mtcomm.2020.101238.
- [170] Zhang X, Liang JS, Li JG, Zeng YN, Hao SJ, Liu PY, et al. The properties characterization and strengthening-toughening mechanism of Al<sub>2</sub>O<sub>3</sub>-CA<sub>6</sub>-MA-Ni multi-phase composites prepared by adding calcined dolomite. Mater Char 2022;186:111810. https://doi.org/10.1016/ j.matchar.2022.111810.
- [171] Chai JL, Zhu Y Bin, Shen TL, Liu YW, Niu LJ, Li SF, et al. Assessing fracture toughness in sintered Al<sub>2</sub>O<sub>3</sub>–ZrO<sub>2</sub>(3Y)– SiC ceramic composites through indentation technique. Ceram Int 2020;46:27143–9. https://doi.org/10.1016/ j.ceramint.2020.07.194.
- [172] Meyers MA, Mishra A, Benson DJ. Mechanical properties of nanocrystalline materials. Prog Mater Sci 2006;51:427-556. https://doi.org/10.1016/j.pmatsci.2005.08.003.
- [173] Hu J, Shi YN, Sauvage X, Sha G, Lu K. Grain boundary stability governs hardening and softening in extremely fine nanograined metals. Science 2017;355:1292–6. https:// doi.org/10.1126/science.aal5166.
- [174] Holleck H, Schier V. Multilayer PVD coatings for wear protection. Surf Coat Technol 1995;76:328–36. https:// doi.org/10.1016/0257-8972(95)02555-3.
- [175] Cheng WJ, Wang JJ, Liu P, Ma X, Zhang K, Ma FC, et al. Effects of Y addition on the microstructures and mechanical behavior of ZrO<sub>x</sub>N<sub>y</sub>/V<sub>2</sub>O<sub>3</sub>-Y nano-multilayered films. Mater Sci Eng, A 2023;864:144555. https://doi.org/ 10.1016/j.msea.2022.144555.
- [176] Shuai JT, Zuo X, Wang ZY, Guo P, Xu BB, Zhou J, et al. Comparative study on crack resistance of TiAlN monolithic and Ti/TiAlN multilayer coatings. Ceram Int 2020;46:6672–81. https://doi.org/10.1016/ j.ceramint.2019.11.155.
- [177] Lee S, Ghaffarian H, Kim W, Lee T, Han SM, Ryu S, et al. A study on dislocation mechanisms of toughening in Cugraphene nanolayered composite. Nano Lett 2022;22:188–95. https://doi.org/10.1021/ acs.nanolett.1c03599.
- [178] Liu R, Hou XS, Yang SY, Chen C, Mao YR, Wang S, et al. The effect of bonding temperature on the bending behaviors and toughening mechanism of W/(Ti/Ta/Ti) multilayer composites prepared by field activated sintering technique. Mater Char 2021;172:110875. https://doi.org/10.1016/ j.matchar.2021.110875.
- [179] Zhou SH, Kuang TC, Qiu ZG, Zeng DC, Zhou KS. Microstructural origins of high hardness and toughness in cathodic arc evaporated Cr-Al-N coatings. Appl Surf Sci 2019;493:1067–73. https://doi.org/10.1016/ j.apsusc.2019.07.051.
- [180] Purandare YP, Robinson GL, Ehiasarian AP, Hovsepian PE. Investigation of High Power Impulse Magnetron Sputtering deposited nanoscale CrN/NbN multilayer coating for tribocorrosion resistance. Wear 2020;452–453:203312. https://doi.org/10.1016/j.wear.2020.203312.
- [181] Hahn R, Bartosik M, Soler R, Kirchlechner C, Dehm G, Mayrhofer PH. Superlattice effect for enhanced fracture

- toughness of hard coatings. Scripta Mater 2016;124:67–70. https://doi.org/10.1016/j.scriptamat.2016.06.030.
- [182] Li Z, Liu CH, Chen QS, Yang JJ, Liu JM, Yang HY, et al. Microstructure, high-temperature corrosion and steam oxidation properties of Cr/CrN multilayer coatings prepared by magnetron sputtering. Corrosion Sci 2021;191:109755. https://doi.org/10.1016/j.corsci.2021.109755.
- [183] Jin SX, Liu N, Zhang S, Li DJ. The simulation of interface structure, energy and electronic properties of TaN/ReB<sub>2</sub> multilayers using first-principles. Surf Coat Technol 2017;326:417–23. https://doi.org/10.1016/ j.surfcoat.2016.11.068.
- [184] Houska J, Rezek J, Cerstvy R. Dependence of the ZrO2 growth on the crystal orientation: growth simulations and magnetron sputtering. Appl Surf Sci 2022;572:151422. https://doi.org/10.1016/j.apsusc.2021.151422.
- [185] Sharma S. Molecular dynamics simulation of ceramic matrix composites using biovia materials studio, LAMMPS, and GROMACS. Elsevier; 2019. https://doi.org/10.1016/B978-0-12-816954-4.00005-X.
- [186] Zhang N, Asle Zaeem M. Competing mechanisms between dislocation and phase transformation in plastic deformation of single crystalline yttria-stabilized tetragonal zirconia nanopillars. Acta Mater 2016;120:337–47. https:// doi.org/10.1016/j.actamat.2016.08.075.
- [187] Zhou XY, Yu XX, Jacobson D, Thompson GB. A molecular dynamics study on stress generation during thin film growth. Appl Surf Sci 2019;469:537–52. https://doi.org/ 10.1016/j.apsusc.2018.09.253.
- [188] Stroet M, Sanderson S, Sanzogni AV, Nada S, Lee T, Caron B, et al. Py thin film: automated molecular dynamics simulation protocols for the generation of thin film morphologies. J Chem Inf Model 2023;63:2–8. https://doi.org/10.1021/acs.jcim.2c01334.
- [189] Ding SB, Wang XQ. Strain rate and temperature effects on the mechanical properties of TiN/VN composite: molecular dynamics study. J Alloys Compd 2020;814:152151. https:// doi.org/10.1016/j.jallcom.2019.152151.
- [190] Koutná N, Löfler L, Holec D, Chen Z, Zhang Z, Hultman L, et al. Atomistic mechanisms underlying plasticity and crack growth in ceramics: a case study of AlN/TiN superlattices. Acta Mater 2022;229. https://doi.org/10.1016/ j.actamat.2022.117809.
- [191] Chen Z, Zheng Y, Löfler L, Bartosik M, Nayak GK, Renk O, et al. Atomic insights on intermixing of nanoscale nitride multilayer triggered by nanoindentation. Acta Mater 2021;214:117004. https://doi.org/10.1016/ j.actamat.2021.117004.
- [192] Xing HR, Hu P, Li SL, Zuo YG, Han JY, Hua XJ, et al. Adsorption and diffusion of oxygen on metal surfaces studied by firstprinciple study: a review. J Mater Sci Technol 2021;62:180–94. https://doi.org/10.1016/j.jmst.2020.04.063.

- [193] Music D, Geyer RW, Schneider JM. Recent progress and new directions in density functional theory based design of hard coatings. Surf Coat Technol 2016;286:178–90. https:// doi.org/10.1016/j.surfcoat.2015.12.021.
- [194] Ullah M, Rana AM, Ahmad E, Raza R, Hussain F, Hussain A, et al. Phenomenological effets of tantalum incorporation into diamond films: experimental and first principle studies. Appl Surf Sci 2016;380:83–90. https://doi.org/10.1016/j.apsusc.2016.02.079.
- [195] Li Y, Xiang C, Chiabrera FM, Yun S, Zhang HW, Kelly DJ, et al. Stacking and twisting of freestanding complex oxide thin films. Adv Mater 2022;34:2203187. https://doi.org/ 10.1002/adma.202203187.
- [196] Hu YZ, Luo LL, Shen HH, Hu SL, Tan ZY, Long XG. Interfacial properties of multilayer graphene and  $\alpha$ -alumina: experiments and simulations. Ceram Int 2022;48:12056–64. https://doi.org/10.1016/j.ceramint.2022.01.064.
- [197] Alaboodi AS, Hussain Z. Finite element modeling of nanoindentation technique to characterize thin film coatings. J King Saud Univ Eng Sci 2019;31:61–9. https://doi.org/ 10.1016/j.jksues.2017.02.001.
- [198] Zhao TK, Zhu JM, Luo J. Study of crack propagation behavior in single crystalline tetragonal zirconia with the phase field method. Eng Fract Mech 2016;159:155–73. https://doi.org/ 10.1016/j.engfracmech.2016.03.035.



Wenjie Cheng is currently a PhD candidate in Prof. Wei Li's group at the School of Materials and Chemistry, University of Shanghai for Science and Technology (USST). His research interests lie in the relationships between phase transition and the mechanical properties of hard nanomultilayered and nanocomposite films.



Wei Li received his PhD degree in materials engineering from Shanghai Jiao Tong University in 2008. He worked as a visiting scholar for one year at the School of Materials, University of Tennessee, USA, in 2016. He is currently a professor at the School of Materials and Chemistry, University of Shanghai for Science and Technology. His research interests include nanostructured super hard films, biomedical materials, high entropy alloy material and their application.